NASA/CR—2001-210611

Task 2—Flow Solution for Advanced Separate Flow Nozzles Response A: Structured Grid Navier-Stokes Approach

D.C. Kenzakowski, J. Shipman, and S.M. Dash
Combustion Research and Flow Technology, Inc., Dublin, Pennsylvania

April 2001

The NASA STI Program Office . . . in Profile

Since its founding, NASA has been dedicated to the advancement of aeronautics and space science. The NASA Scientific and Technical Information (STI) Program Office plays a key part in helping NASA maintain this important role.

The NASA STI Program Office is operated by Langley Research Center, the Lead Center for NASA's scientific and technical information. The NASA STI Program Office provides access to the NASA STI Database, the largest collection of aeronautical and space science STI in the world. The Program Office is also NASA's institutional mechanism for disseminating the results of its research and development activities. These results are published by NASA in the NASA STI Report Series, which includes the following report types:

- TECHNICAL PUBLICATION. Reports of completed research or a major significant phase of research that present the results of NASA programs and include extensive data or theoretical analysis. Includes compilations of significant scientific and technical data and information deemed to be of continuing reference value. NASA's counterpart of peer-reviewed formal professional papers but has less stringent limitations on manuscript length and extent of graphic presentations.

- TECHNICAL MEMORANDUM. Scientific and technical findings that are preliminary or of specialized interest, e.g., quick release reports, working papers, and bibliographies that contain minimal annotation. Does not contain extensive analysis.

- CONTRACTOR REPORT. Scientific and technical findings by NASA-sponsored contractors and grantees.

- CONFERENCE PUBLICATION. Collected papers from scientific and technical conferences, symposia, seminars, or other meetings sponsored or cosponsored by NASA.

- SPECIAL PUBLICATION. Scientific, technical, or historical information from NASA programs, projects, and missions, often concerned with subjects having substantial public interest.

- TECHNICAL TRANSLATION. English-language translations of foreign scientific and technical material pertinent to NASA's mission.

Specialized services that complement the STI Program Office's diverse offerings include creating custom thesauri, building customized data bases, organizing and publishing research results . . . even providing videos.

For more information about the NASA STI Program Office, see the following:

- Access the NASA STI Program Home Page at ***http://www.sti.nasa.gov***

- E-mail your question via the Internet to help@sti.nasa.gov

- Fax your question to the NASA Access Help Desk at 301–621–0134

- Telephone the NASA Access Help Desk at 301–621–0390

- Write to:
  NASA Access Help Desk
  NASA Center for AeroSpace Information
  7121 Standard Drive
  Hanover, MD 21076

NASA/CR—2001-210611

Task 2—Flow Solution for Advanced Separate Flow Nozzles Response A: Structured Grid Navier-Stokes Approach

D.C. Kenzakowski, J. Shipman, and S.M. Dash
Combustion Research and Flow Technology, Inc., Dublin, Pennsylvania

Prepared under Contract NAS3–99098

National Aeronautics and
Space Administration

Glenn Research Center

April 2001

Available from

NASA Center for Aerospace Information
7121 Standard Drive
Hanover, MD 21076
Price Code: A04

Available electronically at http://gltrs.grc.nasa.gov/GLTRS

PREFACE

In 1995, NASA GRC initiated efforts to meet the US industry's rising need to develop jet noise technology for separate flow nozzle exhaust systems. Such technology would be applicable to long-range aircraft using medium to high by-pass ratio engines. With support from the Advanced Subsonic Technology Noise Reduction program, these efforts resulted in the formulation of an experimental study, the Separate Flow Nozzle Test (SFNT). SFNT's objectives were to develop a data base on various by-pass ratio nozzles, screen quietest configurations and acquire pertinent data for predicting the plume behavior and ultimately its corresponding jet noise. The SFNT was a team effort between NASA GRC's various divisions, NASA Langley, General Electric, Pratt&Whitney, United Technologies Research Corporation, Allison Engine Company, Boeing, ASE FluiDyne, MicroCraft, Eagle Aeronautics and Combustion Research and Flow Technology Incorporated.

SFNT found several exhaust systems providing over 2.5 EPNdB reduction at take-off with less than 0.5% thrust loss at cruise with simulated flight speed of 0.8 Mach. Please see the following SFNT related reports: Saiyed, et al. (NASA/TM—2000-209948), Saiyed, et al. (NASA/CP—2000-210524), Low, et al. (NASA/CR—2000-210040), Janardan et al. (NASA/CR—2000-210039), Bobbitt, et al. (NASA/CR—201-210706) and Kenzakowski et al. (NASA/CR—2001-210611.).

I wish to thank the entire SFNT team of nearly 50 scientists, engineers, technicians and programmers involved in this project. SFNT would have fallen well short of its goals without their untiring support, dedication to developing the jet noise technology.

Naseem Saiyed
SFNT Research Engineer

Task 2 – Flow Solution for Advanced Separate Flow Nozzles Response A: Structured Grid Navier-Stokes Approach

Final Technical Report

1.0 OVERVIEW

This report describes the work performed under NASA/Glenn Research Center Contract No. NAS3-99098 supporting technology for reducing aircraft noise caused by the exhaust plume from separate flow nozzles. A series of detailed CFD plume flowfield simulations was performed to better understand the flowfield features introduced by passive noise reduction devices and to predict the resulting mean and turbulent flowfield quantities. The nozzle configurations studied included a baseline (axisymmetric) design and two modifications to the baseline using a pre-determined arrangement of chevrons and tabs attached at the core nozzle exit. The flowfield domain extended from upstream of the nozzle exit to approximately 25 fan diameters downstream to assess core/fan mixing enhancement. The resulting mean and turbulent flowfield quantities were to be then compared with experimental measurements performed at the same operating conditions. The numerical solutions were also used as inputs to the MGB [1] code for assessing the Reynolds-averaged Navier-Stokes (RANS) methodology in predicting the observed jet noise level reduction resulting from vortical mixing enhancement.

An overview of the nozzle configurations studied is displayed in Figure 1. The baseline configuration consists of an axisymmetric laboratory scale separate flow nozzle with an external plug. The chevron assembly is characterized by six evenly distributed sets of two chevrons that alternately point inward toward the plume axis and outward by the same relative angle with respect to the core cowl exit. The tabs considered are of "delta" design arranged in an alternating pattern such that six are inclined by 30° into the core stream, six are inclined by 30° into the fan stream, and twelve tabs remain aligned (i.e., neutral) with nozzle exit convergence angle. For a RANS flowfield simulation, both the tab and chevron arrangements allow for 30-degree symmetry to be assumed for the computational domain. In all simulations, strut and pylon interference effects have been neglected, and the inflow profiles do not include boundary layer effects. The results discussed below are "first-pass;" a baseline $k\varepsilon$ turbulence model (no axisymmetric correction or non-linear extensions) has been used, and a constant turbulent Prandtl of 0.7 has been employed based on previous plume modeling experiences. The flowfield solutions have been solved on grids of comparable axial and radial resolution. The results and comparisons are discussed below.

Two sets of flowfield conditions were used for each nozzle in these studies. The first set, specified in Table I, corresponded to conditions to be run at the NASA/Langley Jet Noise Laboratory (JNL), where mean and fluctuating flowfield quantities were to be measured for comparison with numerical predictions. These comparisons were to provide useful information in turbulence model assessment for jet noise prediction. Unfortunately, these experimental results were not obtained during

the period of performance of this task. As an alternative to turbulence model validation and rectification with the JNL data, the three nozzle/plume flowfields were also run at conditions for which mean flow and acoustic measurements were previously obtained at the NASA/Glenn jet noise facility; these flowfield conditions are listed in Table II. The resulting CFD mean and turbulent flowfields were then delivered to NASA/Glenn for data comparison. Qualitatively, both engine conditions produced similar mixing features for a given nozzle configuration. Therefore, for brevity, this report will focus on discussing the flowfield comparisons for the Power Point 22 operating conditions. For completeness, radial profile comparisons at stations of interest to NASA/Glenn have been included as an appendix to this report. Results of the Power Point 21 flowfield calculations will be presented once experimental comparisons are made available.

Table I. Power Point 22 Flowfield Conditions For Assessing Jet Noise Reduction

	Core	Fan	Freestream
Total Pressure (atm)	1.480	1.695	1.035
Total Temperature (K)	794.44	333.33	298.87

Freestream Static Pressure = 14.4 psia (0.98 atm)
Freestream Static Temperature = 294.26 K
Freestream Mach Number = 0.28

Table II. Power Point 21 Flowfield Conditions For Assessing Jet Noise Reduction

	Core	Fan	Freestream
Total Pressure (atm)	1.650	1.800	1.035
Total Temperature (K)	833.33	333.33	298.87

Freestream Static Pressure = 14.4 psia (0.98 atm)
Freestream Static Temperature = 294.26 K
Freestream Mach Number = 0.28

2.0 NUMERICAL PROCEDURE

The internal and jet plume flowfields for a baseline axisymmetric (Model Designation 3BB) and two advanced 3D nozzles with chevrons (Model $3A_{12}B$) nozzle and tabs (Model $3T_{24}B$) were calculated using the CRAFT structured grid Navier-Stokes code. The CRAFT code is a finite-volume, fully

implicit, Roe/TVD solver that has been used extensively for jet simulations studying noise reduction concepts and aircraft plume IR signatures [2-5]. A number of capabilities exist in CRAFT that make it suitable for advanced jet simulation studies, and these are highlighted below. For all simulations a perfect gas equation of state (γ=1.4) and a constant turbulent Prandtl number of 0.7 were assumed, and a baseline kε turbulence model was used. Sensitivity of the flowfield features to turbulence modeling extensions, such as the Gatski/Speziale non-linear turbulence model, centerline corrections, and variable Prandtl number, were not considered in the present effort but may be important to consider in future studies after data comparisons are made.

The grid blanking methodology in CRAFT increases its versatility for flowfield problems involving complex geometries. This feature works in conjunction with the implicit ADI procedure for inverting the matrix arrays in the direction of the implicit sweep. Grid blanking also facilitates structured mesh generation by allowing the grids to better conform to the specified geometry and flow direction and minimize "skewness." As an example, a schematic of the grid blanking used for the baseline nozzle flowfield is illustrated in Figure 2. User-specified boundary conditions along internal and external grid surfaces allow for automatic construction of patches, or sweeps, in each computational direction. Moreover, wall boundaries do not need to coincide with inter-block boundaries. This allows for a more generalized placement of interior boundary conditions away from regions that are likely to interfere with shear layer development and restrict time advancement.

The boundary layer region is an important aspect of the nozzle flowfield, especially for transonic exhausts. It is therefore important to accurately predict the mass deficit effect of the boundary layer to assess nozzle performance. In addition, boundary layer turbulence can impact the downstream plume shear layer development, especially for the core/fan mixing region where velocity ratios are small. Resolution of the boundary layer flowfield near the wall would require tightly packed grids of high cell aspect ratio, which increases storage and CPU costs (more grid points needed) and often hinders solution convergence due to the small local time steps required. In an effort to reduce the costs for resolving viscous wall effects, a compressible law of the wall model [6] has been implemented in CRAFT and was used for both the axisymmetric and 3D simulations. Wall functions analytically relate surface boundary conditions to points in the inertial sublayer region, where the shear stress is assumed constant. In this study, the grid resolution employed ensured that the first cell location off the wall was less than a y^+ of 25 and a minimum of eight grid points were below a y^+ of 300. This latter constraint was made to provide a reasonable estimate of momentum deficit effects on the flowfield exhaust (e.g.. mass flow rates). For the present studies, adiabatic walls were assumed.

The solution of the 3D nozzle flowfields required nearly three million grid cells for the chevron case and five million cells for the tab case. To boost solution turnaround time, a domain decomposition strategy was employed for distributing the overall computational volume across a user-specified number of processors and running the CRAFT code in parallel via the Message Passing Interface (MPI) library. This domain decomposition procedure allows for linear solution speedup on parallel architectures and operates independently of the patching methodology described above. This feature enables the user to

focus grid construction based on flowfield resolution requirements and not on processor load balancing. This also allows for placement of potential inter-block boundary interference away from regions of shear layer evolution. For the present simulations, sixteen processors were used for the chevron solution, and twenty processors were used for the tab flowfield.

Subsonic conditions were imposed at all inflow boundaries using the specified total pressure and total temperature. For the current simulations, charging station profiles were unavailable, and thus uniform conditions were prescribed at these boundaries.

3.0 COMPUTATIONAL DOMAIN

The entire computational domain consisted of the internal nozzle flowfield, initiated at a location prescribed by NASA/Glenn sufficiently upstream of the core and fan nozzle exits, and the volume of external flow enclosing the downstream plume and associated freestream. The nozzle component surfaces were specified using IGES files obtained from NASA/Glenn, and grid construction was done using GRIDGEN Version 13. The streamwise length of the computational domain extended 25 fan exit diameters downstream of the external plug tip and included the entire jet growth in the radial direction. Both the axisymmetric and 3D chevron grids were constructed with similar wall mesh density to minimize boundary layer resolution effects in the subsequent flowfield comparisons. The axisymmetric grid dimensions were 537x160. An overall view of this mesh and the use of grid blanking for this geometry are shown in Figure 3. Grids were packed radially along all wall surfaces and axially near the fan and core nozzle exits. The axisymmetric grid topology was selected to facilitate comparisons with the chevron flowfield and to provide a good initial flowfield solution for the 3D cases. A similar gridding strategy was used for the chevron case (537x160x40), shown in Figure 4, and the tab case (537x160x60), shown in Figure 5. Figure 6 illustrates the overall flow domain used for the chevron nozzle; the blue outlines in this figure denote the sixteen processor breakup of the domain for parallel execution. Based on the geometric configuration, thirty-degree symmetry was assumed, and Figure 7 illustrates the azimuthal grid density used for resolving cross flow features.

4.0 BASELINE NOZZLE STUDIES

Predicted Mach number contours for the overall axisymmetric solution domain are shown in Figure 8. The peak Mach number at the fan exit is slightly below sonic (0.956). The blunt trailing edge of the external plug produces a small recirculation zone and downstream wake region along the plume axis. Figure 9 shows a close-up view of the Mach number contours in the vicinity of the nozzle. The curvature of the internal wall surfaces near the fan and core exit stations establishes local expansion regions and produces non-uniform Mach number profiles at the exit planes. Figure 10 shows the resulting static pressure flowfield near the nozzle exit, and Figure 11 shows predicted stagnation pressure contours for the overall flowfield, which indicates the mixing extent of the fan stream and freestream. Figure 12 gives a close-up view of the predicted stagnation pressure profile at the core nozzle exit station. At this location the fan flow boundary layer is shown to be slightly thicker than that

of the core. Figure 13 shows contours of the total temperature flowfield and illustrates the relatively slower mixing of the fan and core streams, characteristic of unmodified separate flow nozzles. The turbulent viscosity contours of Figure 14 display the relative levels of turbulent mixing between the three streams. The velocity ratio between the fan and core stream is small; shear layer mixing in this region is consequently slow and results in a long plume core length. The turbulence flowfield is dominated by the fan/freestream mixing; the displayed turbulent viscosity contours must be clipped by an order of magnitude (Figure 14b) to enhance visualization of the fan/core shear layer. The turbulence intensity is a non-dimensional quantity defined for the present comparisons to be the ratio of turbulent kinetic energy to mean kinetic energy:

$$\sqrt{k/q}, \text{ where } q = \frac{1}{2}\left(u^2 + v^2 + w^2\right)$$

This quantity is shown in Figure 15 for the baseline nozzle configuration. Again, this figure illustrates the dominance of the turbulence flowfield by the fan/freestream mixing layer and the small levels of turbulent mixing between the core and fan streams.

5.0 CHEVRON NOZZLE STUDIES

As described above the chevron nozzle is a modification of the baseline design and consists of twelve chevrons alternately deflecting inward and outward along the core cowl lip. This configuration has thirty-degree symmetry, with one symmetry plane slicing through the center of the upward chevron and the other slicing through the center of the downward chevron. The presence of the chevrons significantly changes the plume structure in the near field. As shown in the Mach number, static pressure, and stagnation pressure contours of Figures 16, 17, and 18 respectively, there is a notable difference in the mixing of the core/fan flow in the upward deflected chevron plane versus that in the downward deflected one. The downward deflected chevron allows for penetration of the fan flow into the core stream just downstream of the nozzle exit, while the upward deflected chevron allows for an "injection" of core flow into the fan stream. Overall fan/freestream shear layer mixing does not seem significantly altered by the presence of the chevrons. Total temperature contours, shown in Figure 19, indicate significantly greater mixing of the fan and core flows in the near field. The clipped turbulent viscosity contours of Figure 20 indicate that the fan/freestream mixing layer is still the dominant turbulent region in the plume near field. While the fan/core turbulent viscosity region is slightly broader in the upward chevron plane than was seen for the axisymmetric nozzle, the magnitude levels are approximately the same. This observation is also seen in the turbulence intensity contours of Figure 21.

The enhanced mixing in the near field by the chevrons appears to result from the establishment of large-scale counter-rotating vortices. Figure 22 shows at selected axial locations the cross-flow velocity vectors, which have been colored by the total temperature to better visualize how they affect the

core/fan mixing. These vortices act to "pinch" off regions of core flow, which are then locally mixed out.

6.0 TAB NOZZLE STUDIES

As described above, the tab nozzle is a modification to the baseline design and consists of twenty-four delta tabs arranged in an "upward-neutral-downward-neutral" pattern along the core nozzle exit circumference. As in the chevron nozzle, this configuration contains thirty-degree symmetry, with one plane of symmetry slicing through the center of an upward deflecting tab and the other slicing through the center of a downward tab. Contours have been made in these two planes to help assess the effects of the tabs on the plume structure. Mach number, static pressure, and stagnation pressure contours, shown respectively in Figures 23, 24, and 25, indicate notable differences in the mixing of the core/fan flows due to tab deflection angles. The downward deflected tab allows for penetration of the fan flow into the core stream just downstream of the nozzle exit, while the upward deflected tab allows for an "injection" of core flow into the fan stream. The overall mixing behavior is qualitatively similar to that seen for the chevron nozzle configuration. It is important to note that the stagnation pressure contours indicate that losses occur near the deflected tabs.

Stagnation temperature contours, shown in Figure 26, indicate significant mixing of the core and fan flows in the plume near field. A comparison of total temperature profiles along the plume axis, presented in Figure 27 for the three nozzle configurations, shows that the potential core is dramatically reduced by the presence of the tabs. However, these axial profiles do not completely represent the flowfield mixing, since the dominant vortical mixing in the near field occurs off-axis. A better description of core flow mixing is illustrated in the station-wise integrated flowfield comparisons of Figure 28. Both the tabs and chevrons significantly increase mixing in the plume near-field, with the tabs initially producing a slightly faster rate. Once the vortical regions become fully mixed, overall core flow is significantly reduced, as seen in the large slope change approximately 30 inches downstream of the fan exit.

Figure 29 presents contours of turbulent kinetic energy along the symmetry planes. As in the chevron and baseline cases, the shear layer mixing between the fan and freestream dominates the turbulence field. Peak values for the present study are shown to occur off-axis shortly downstream of the plug tip, followed by a slow decay as the fan/freestream mixing layer approaches the axis. Due to the presence of recirculation zones, high values of turbulent kinetic energy are also seen in the vicinity of the upward and downward penetrating tabs. These turbulent regions do not seem to promote mixing, as evidenced by relatively thin fan/core shear layer and the rapid decay of turbulent kinetic energy in this region.

While the total temperature contours indicate rapid mixing of the core and fan streams by the presence of the selected tab configuration, the flowfield analysis indicates possible areas for improvement. In particular, the relatively large penetration of the tabs into the core and fan streams establishes localized regions of recirculation zones that were not seen in the chevron mixing analysis. Figure 30 shows vectors of velocity colored by stagnation pressure to indicate the losses associated with

the recirculating regions. Figure 31 shows that these zones also produce high levels of turbulent kinetic energy. The turbulent kinetic energy does little to enhance the shear mixing of the core and fan streams and may be a potential source for noise emission, an undesirable feature.

7.0 CHEVRON/BASELINE COMPARISONS

In an effort to gain more insight into the physics of the chevron mixing, comparisons were made at several axial locations between the baseline and chevron plume flowfields. Figure 32 is provided as a reference to physically indicate the location of each station relative to the nozzle assembly. The station numbers represent their respective relative distance from the fan nozzle exit. The stations selected for comparison include locations of interest to NASA/Glenn for future comparisons with experiments as well as supplemental locations upstream of the core plug tip to better identify the developing vortical patterns generated by each design.

Figure 33 compares the total temperature mixing of the axisymmetric nozzle with that using the chevrons. The alternating pairs of upward and downward chevrons establish localized regions of core flow, which are then mixed out by the presence of the cross flow vortices. By X=30, the dominant physics mixing the fan and core streams is shear layer turbulence, which is relatively weak. Despite the rapid mixing in the plume near field, the core stream for the chevron case is not fully mixed until further downstream. In fact, it appears that the centerline rates of temperature decay are similar in the farfield for the two configurations. Figure 34 compares the turbulent kinetic energy contours at the same axial locations. The shape of the shear layer between the fan and core streams appears distorted by the chevrons; however, the overall width of the shear layer is not significantly altered. Figure 34 also indicates the presence of local turbulence intensity peaks within the fan/freestream shear layer due to the flowfield distortion. These peaks produce slight distortions (a non-circular shape) in this region downstream due to a localized increase in the fan and freestream turbulent mixing. Peak levels of turbulent kinetic energy to not appear in the baseline plume until further downstream (X=80), where the primary shear layer reaches the axis.

8.0 TAB-CHEVRON FLOWFIELD COMPARISONS

In an effort to gain more insight into the physics associated with the tab and chevron mixing, plume flowfield comparisons were made at the same axial locations used above. Figure 35 compares the total temperature mixing the chevron and tab nozzle flowfields. The upward and downward pattern of the chevrons establishes localized regions of core flow, which are then mixed out by the presence of counter-rotating vorticies. The tab configuration establishes a more complex vortex pattern. The effect of the "neutral" tabs between the "penetrating" ones is to establish radial vortex "pairs," which promote faster mixing than the chevrons. This can be seen most clearly in the locations downstream of the plug tip; at X=24 inches, the core flow is almost completely mixed for the tab case, while the chevron mixing is not completed until much further downstream (X=60). Figure 36 compares contours of stagnation pressure for the two designs. The effects of tab-induced recirculation are evidenced by the lower values

of stagnation pressure in the vortex core regions. Figure 37 compares contours of turbulent kinetic energy at the same axial locations. The distortions of the fan/core shear layers highlight the differing vortex roll-up patterns established by the chevrons and tabs. Peak values of turbulence in the fan/freestream shear layer are similar for the two cases, although high values of turbulent kinetic energy persist farther downstream for the chevron case.

9.0 REFERENCES

[1] Mani, R., Gliebe, P.R., and Balsa, T.F., "High Velocity Jet Noise Source Location and Reduction," Federal Aviation Administration, Task 2, FAA-RD-76-79-II, Cincinnati, OH, May 1978.

[2] Dash, S.M., Kenzakowski, D.C., Perrell, E.R., Cavallo, P.A., Chidambaram, N., and Sinha, N., "Advances in Simulation of Passive Jet Noise Reduction," AIAA-98-2268 4th AIAA/CEAS Joint Aeroacoustics Conference, Toulouse, France, June 2–4, 1998.

[3] Sinha, N., Chidambaram, N., Dash, S.M., and Seiner, J.M., "Large Eddy Simulation of Laboratory, Subsonic Jets," AIAA-98-2355, 4th AIAA/CEAS Joint Aeroacoustics Conference, Toulouse, France, June 2–4, 1998.

[4] Cavallo, P.A., Kenzakowski, D.C., and Dash, S.M., "Axisymmetric Flowfield Analysis of the F414-400 Turbofan and Exhaust Plumes," Final Report, Combustion Research and Flow Technology, Inc., Report No. CRAFTR-10/97.014, October 1997.

[5] Dash, S.M., Kenzakowski, D.C., and Seiner, J.M., "Advanced Computational Simulation of Plume/Aircraft Wake Nearfield Interactions and Data Comparisons," NASA AEAP Annual Mtg., Virginia Beach, VA, April 23-28, 1995.

[6] Kenzakowski, D.C., and York, B.J., "Inclusion of Compressible Wall Function Methodology Into CRAFT Navier-Stokes Code; Task 3, part 2: Wall Function," CRAFTR-2/97.003.

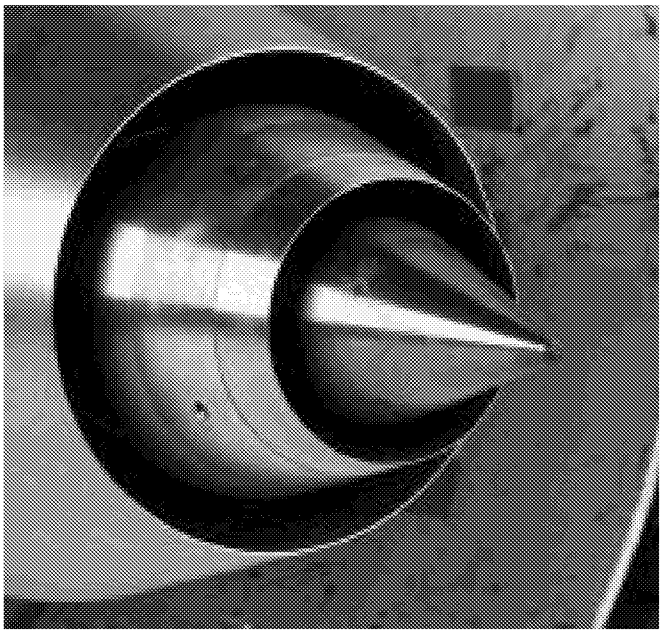

(a) baseline

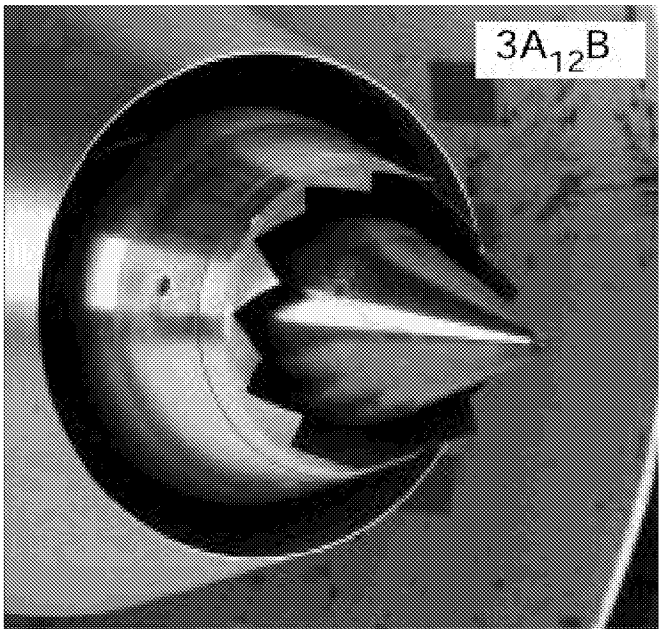

(b) chevron

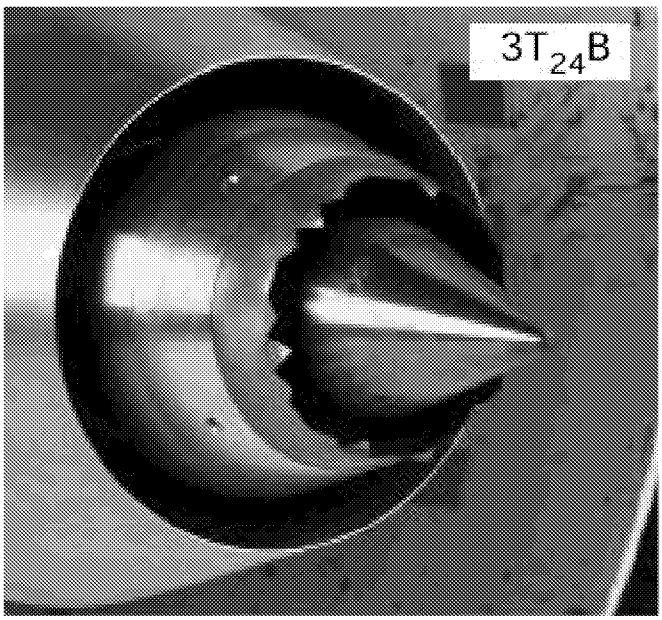

(c) tab

Figure 1. Overview of AST nozzle configurations studied.

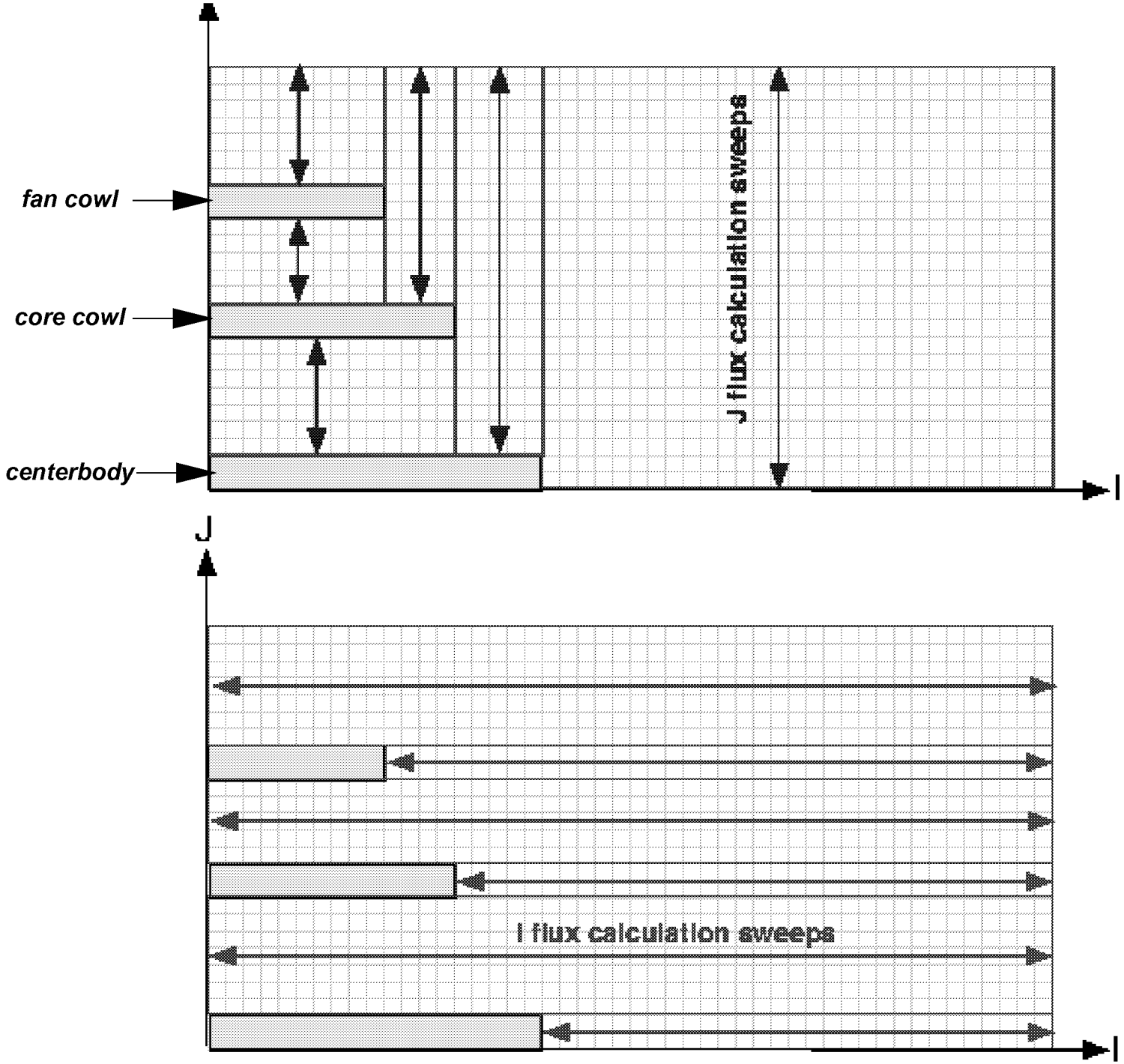

Figure 2. Illustration of patching methodology of CRAFT code as applied to baseline nozzle configuration.

Figure 3. Baseline axisymmetric grid: (a) overview and (b) close–up of nozzle region.

Figure 4. Close up view of chevron grid in region of nozzle.

Figure 5. Close–up view of the tab grid in region of nozzle.

Figure 6. Symmetry plane of computational grid used for chevron flowfield simuations. Blue lines denote inter−processor boundary locations for parallelization.

Figure 7. Axial cuts of chevron grid to illustrate azimuthal resolution.

Figure 8. Mach number contours for axisymmetric nozzle configuration.

Figure 9. Mach number contours showing boundary layer and curvature effects in nozzle flowfield region.

Figure 10. Static pressure contours for internal nozzle and plume exhaust of axisymmetric configuration.

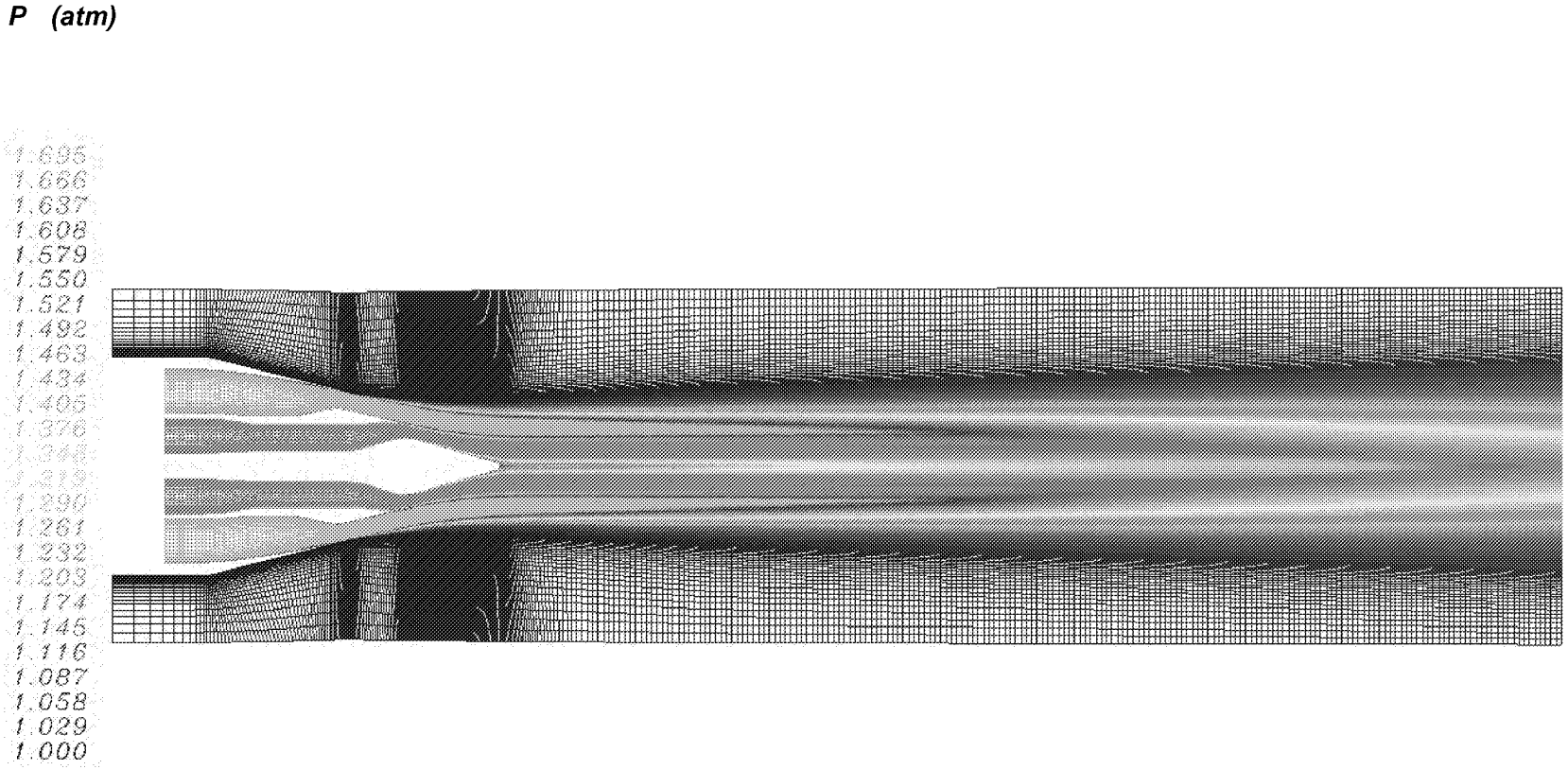

Figure 11. Stagnation pressure contours for internal nozzle and plume exhaust of axisymmetric configuration.

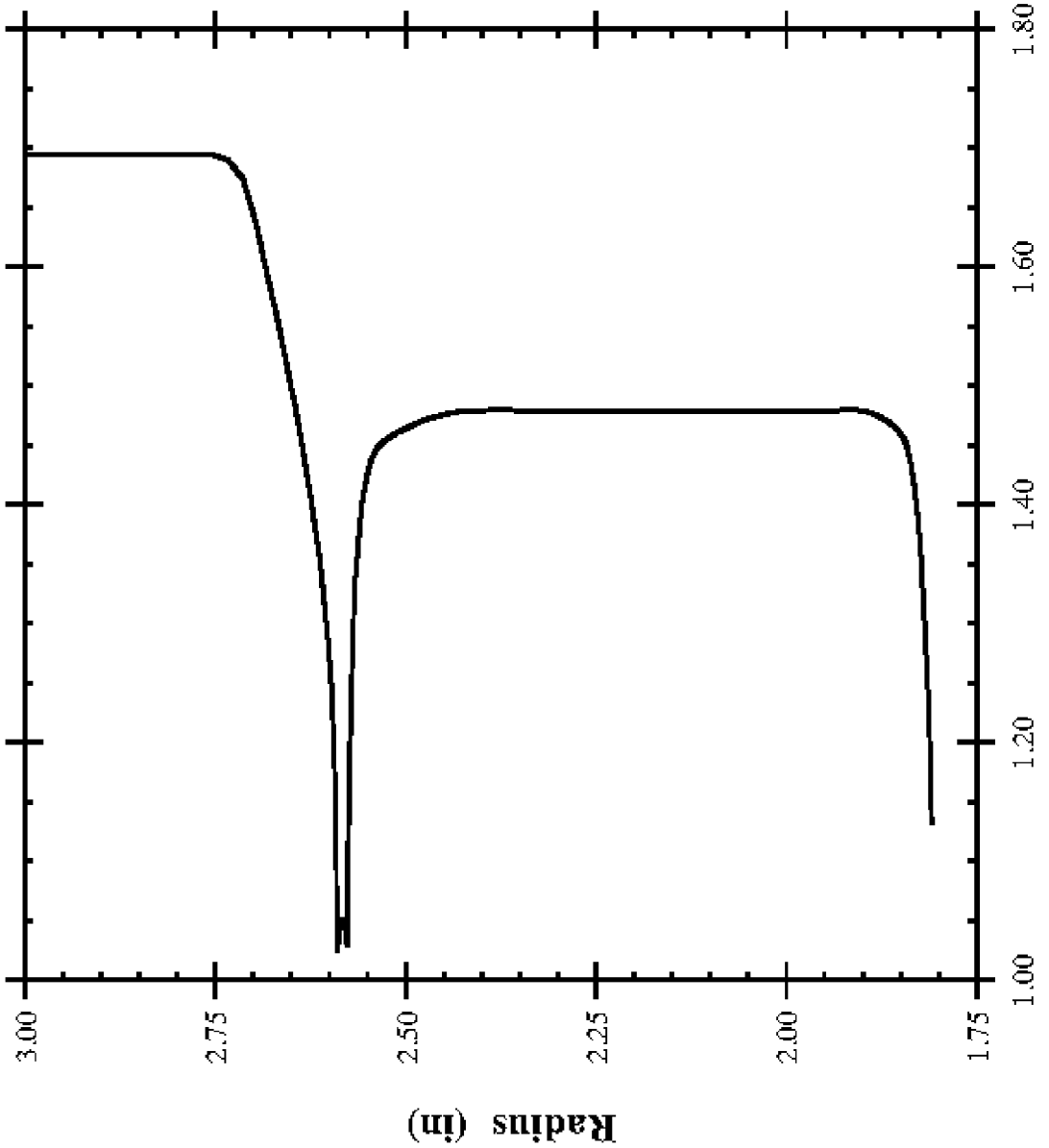

Figure 12. Stagnation pressure profile at core exit station for baseline external plug configuration.

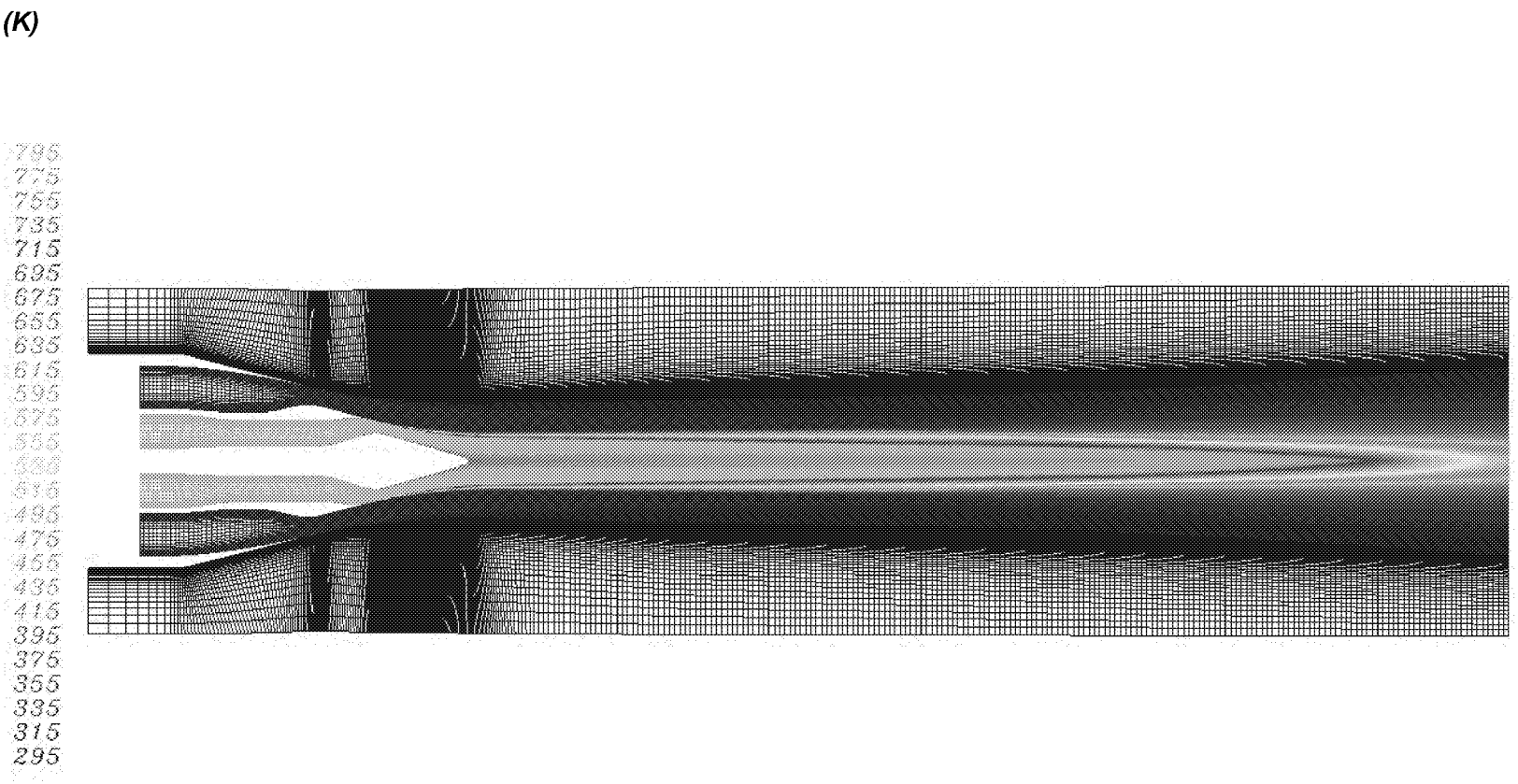

Figure 13. Stagnation temperature contours for internal nozzle and exhaust plume of axisymmetric configuation.

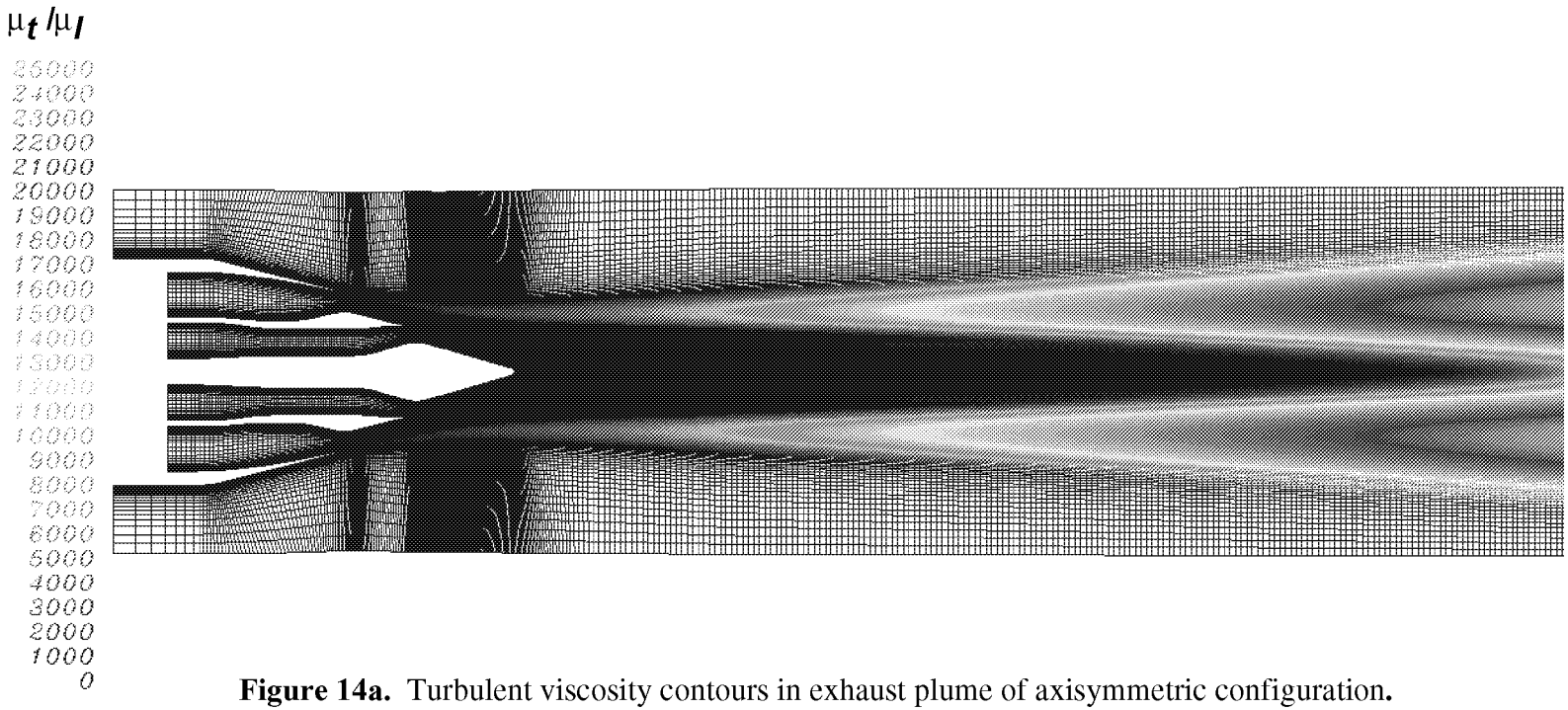

Figure 14a. Turbulent viscosity contours in exhaust plume of axisymmetric configuration.

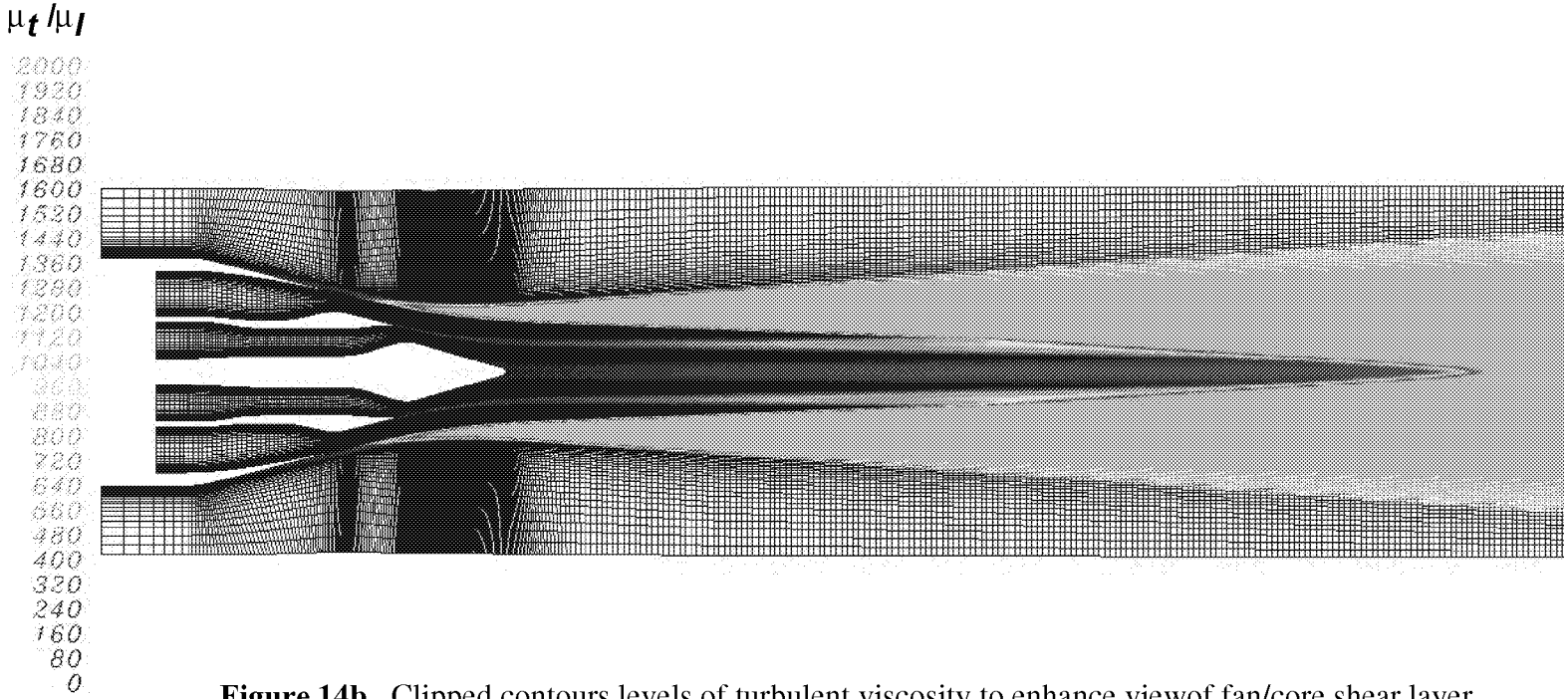

Figure 14b. Clipped contours levels of turbulent viscosity to enhance viewof fan/core shear layer.

Figure 15. Turbulence Intensity Contours for internal nozzle and exhaust plume for axisymmetric configuration.

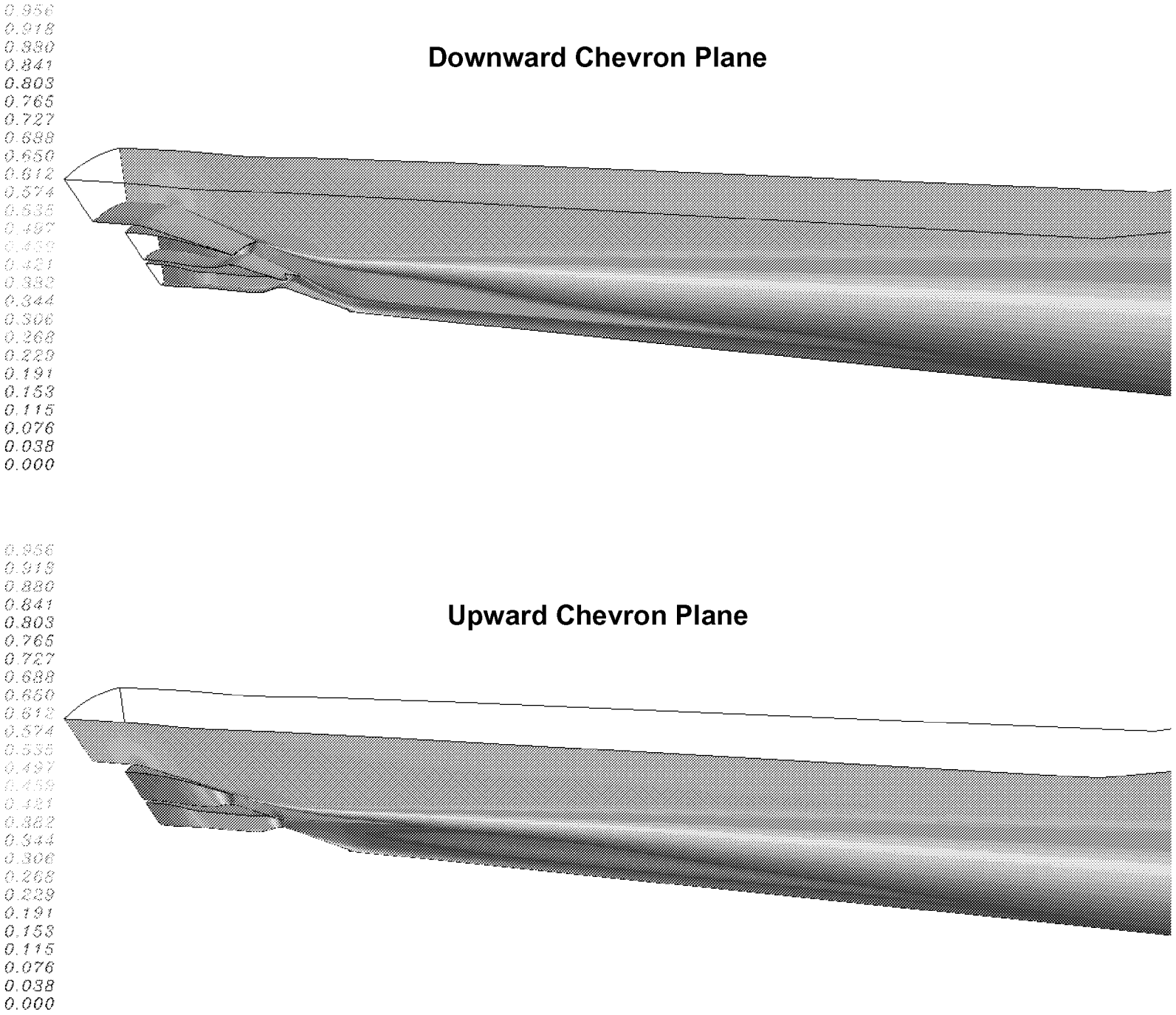

Figure 16. Mach number contours along symmetry planes for chevron nozzle configuration.

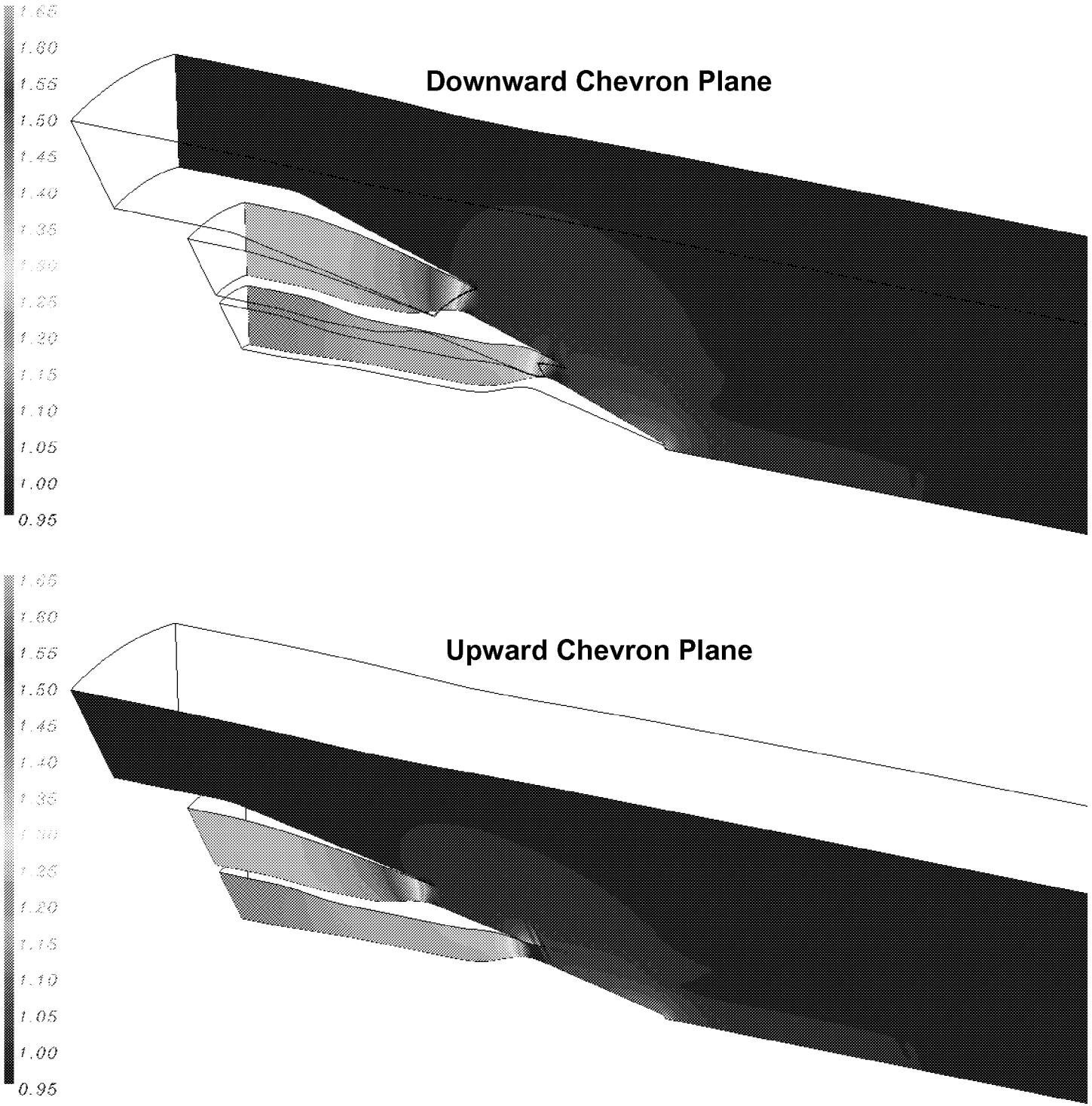

Figure 17. Static pressure contours along symmetry planes for chevron nozzle configuration.

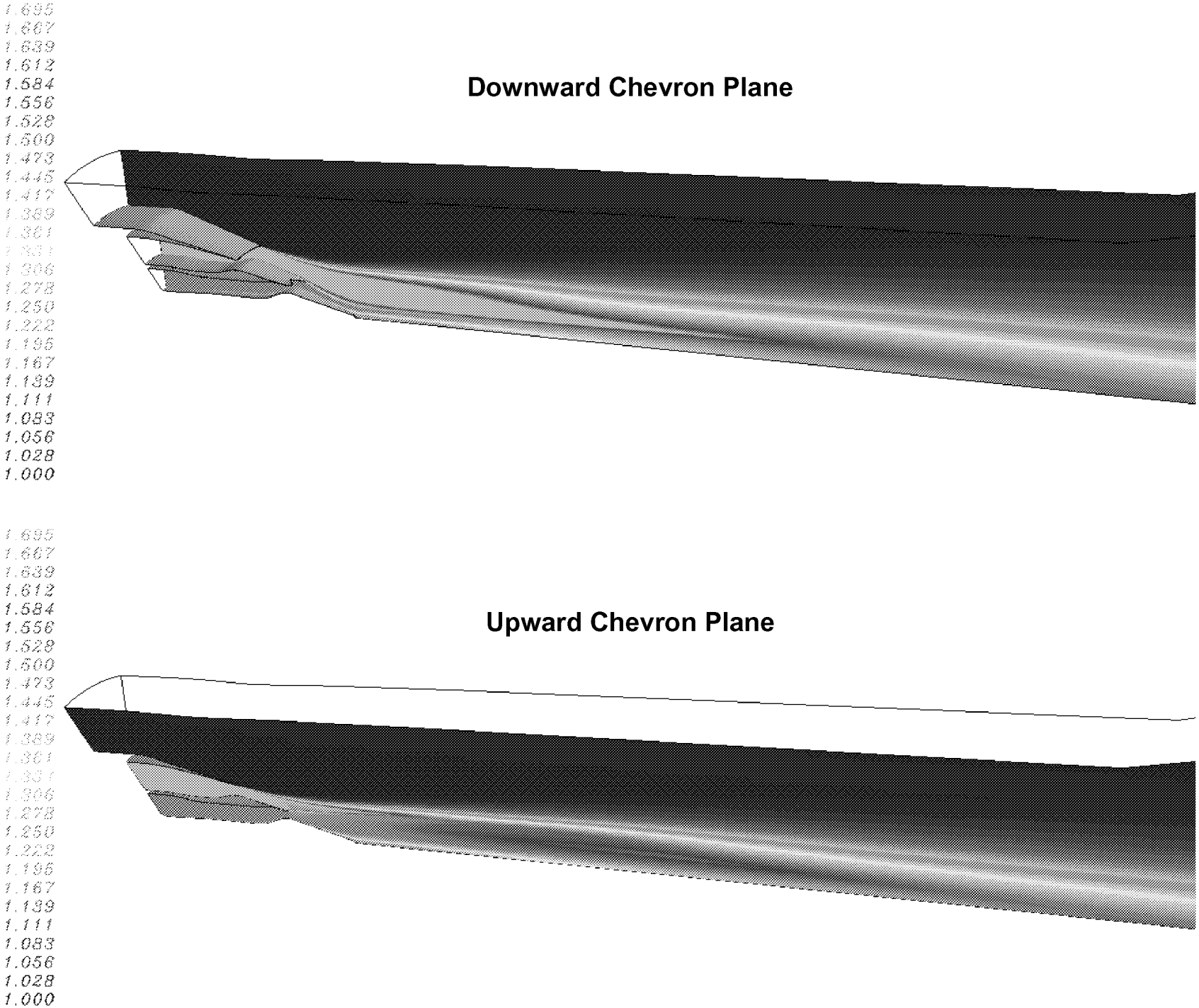

Figure 18. Stagnation pressure contours along symmetry planes for chevron nozzle configuration.

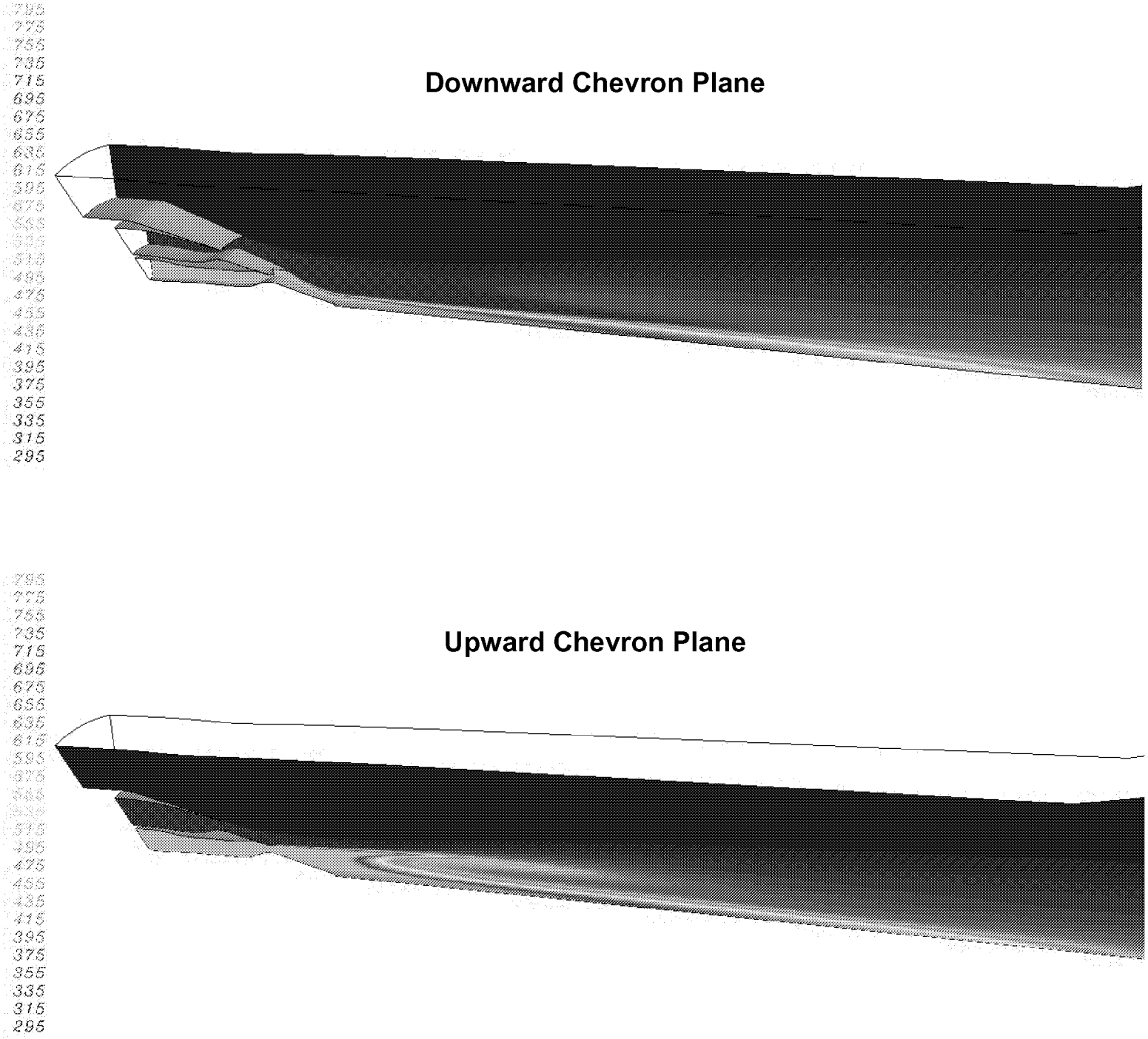

Figure 19. Stagnation temperature contours along symmetry planes for chevron nozzle configuration.

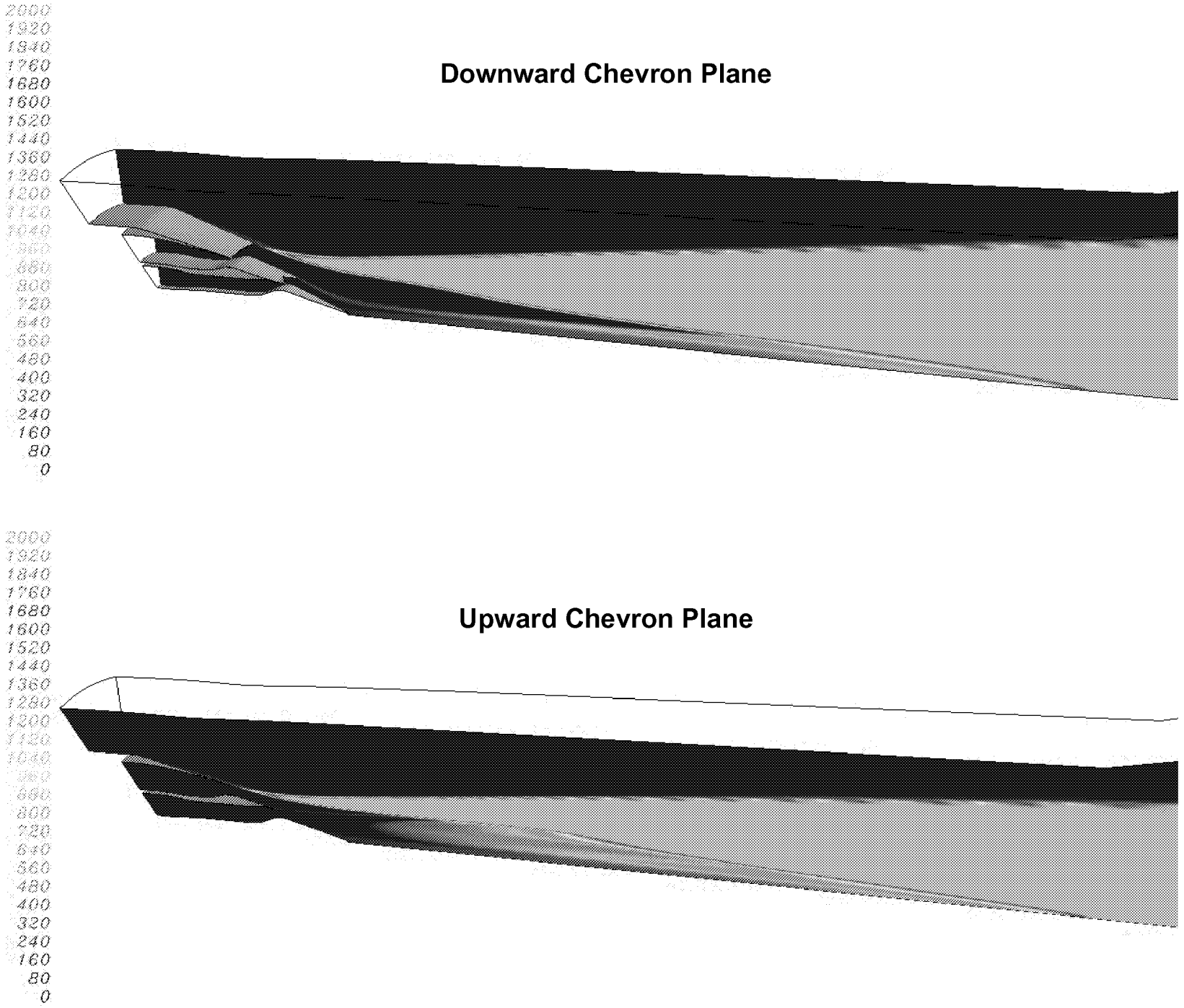

Figure 20. Turbulent visosity contours (clipped) along symmetry planes for chevron nozzle configuration.

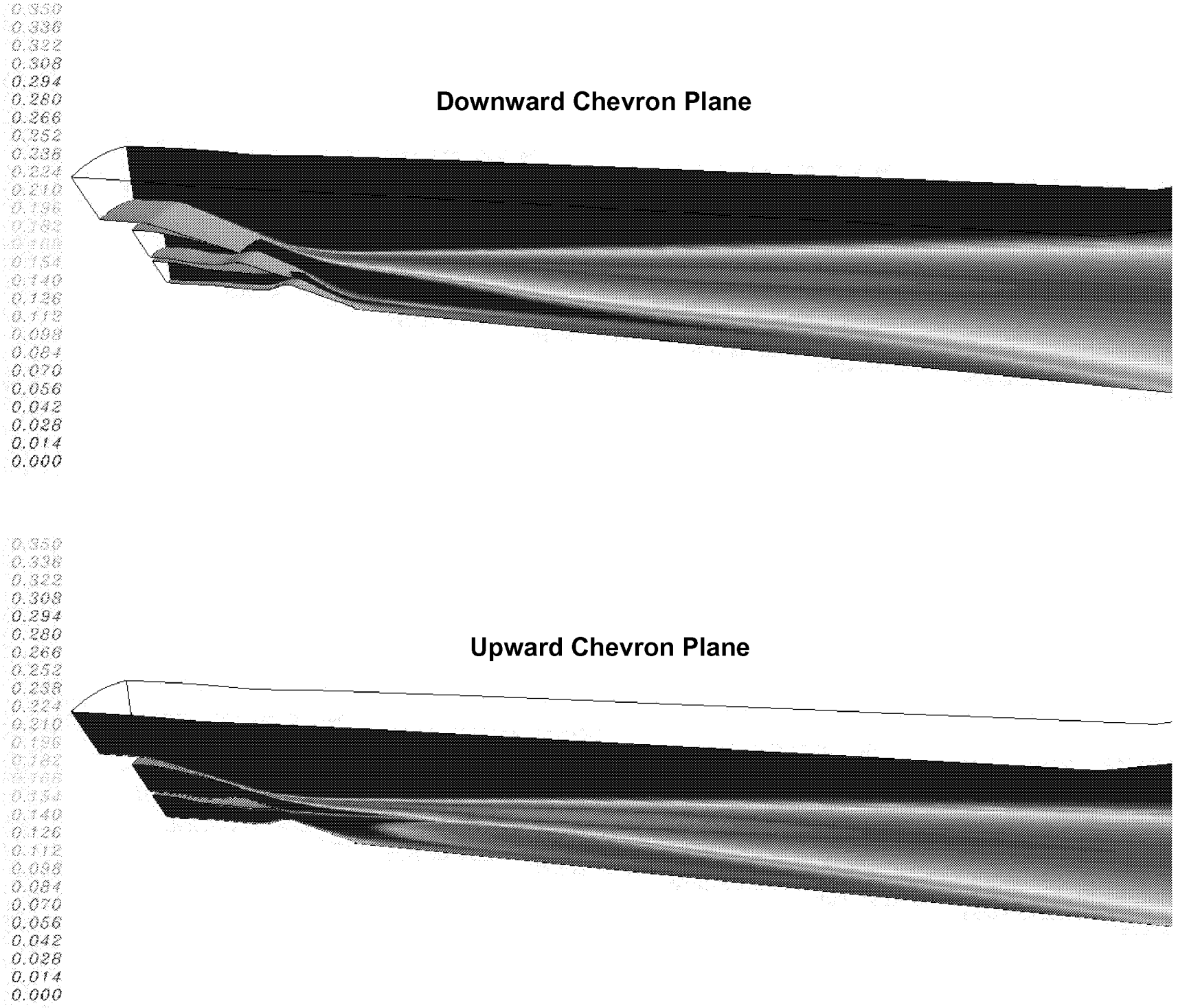

Figure 21. Turbulence intensity contours along symmetry planes for chevron nozzle configuration.

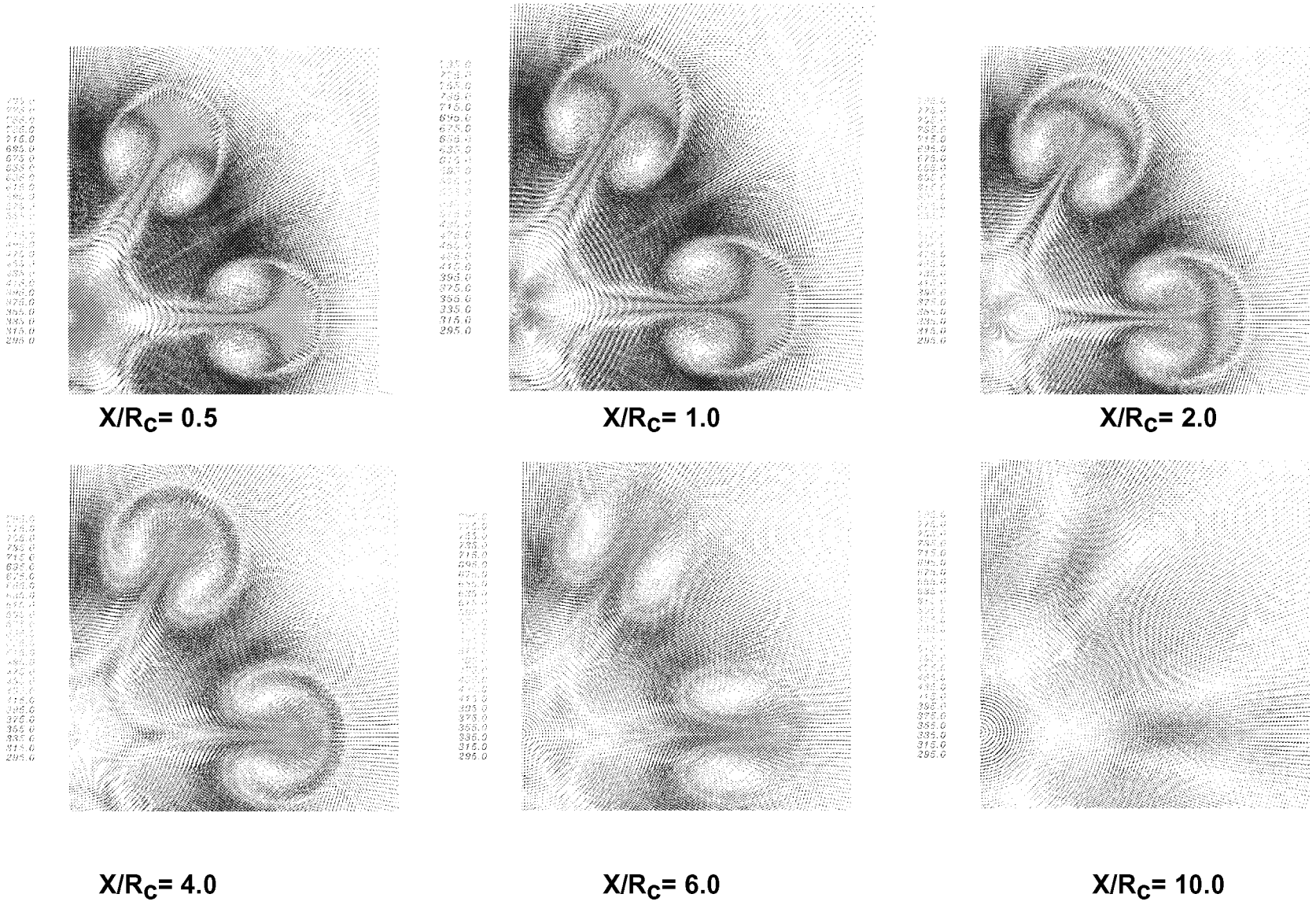

Figure 22. Crossflow velocity vectors colored by total temperature at selected axial stations of chevron plume flowfield.

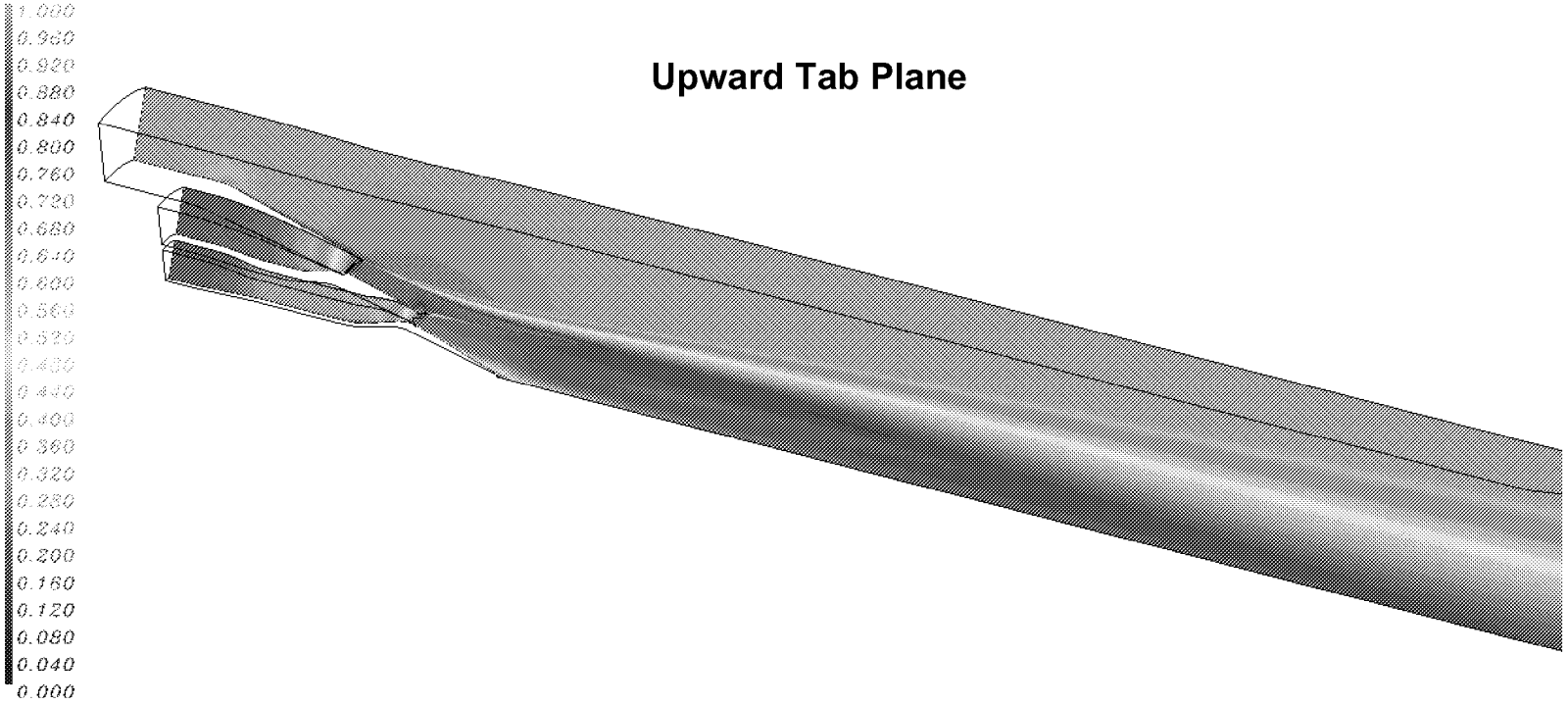

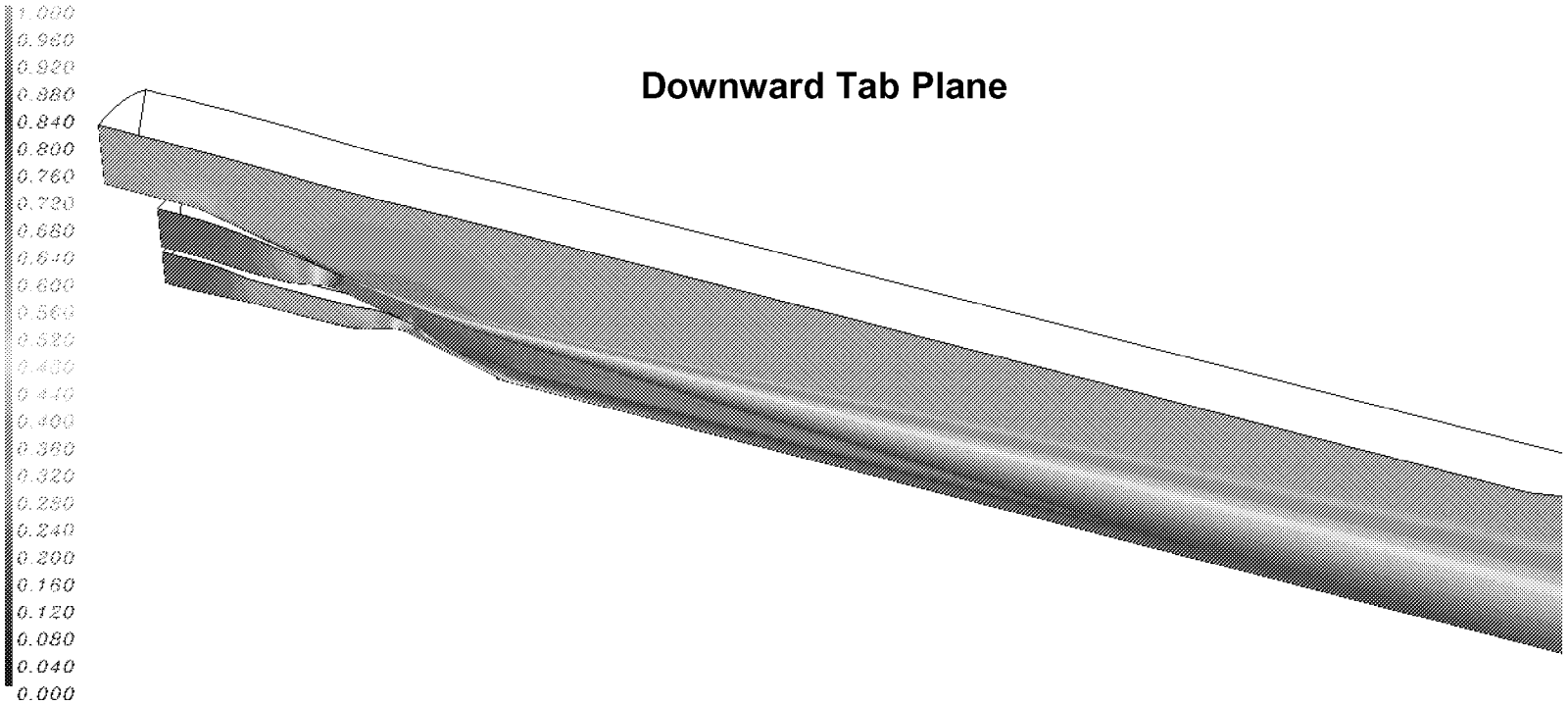

Figure 23. Mach number contours along symmetry planes for tab nozzle configuration.

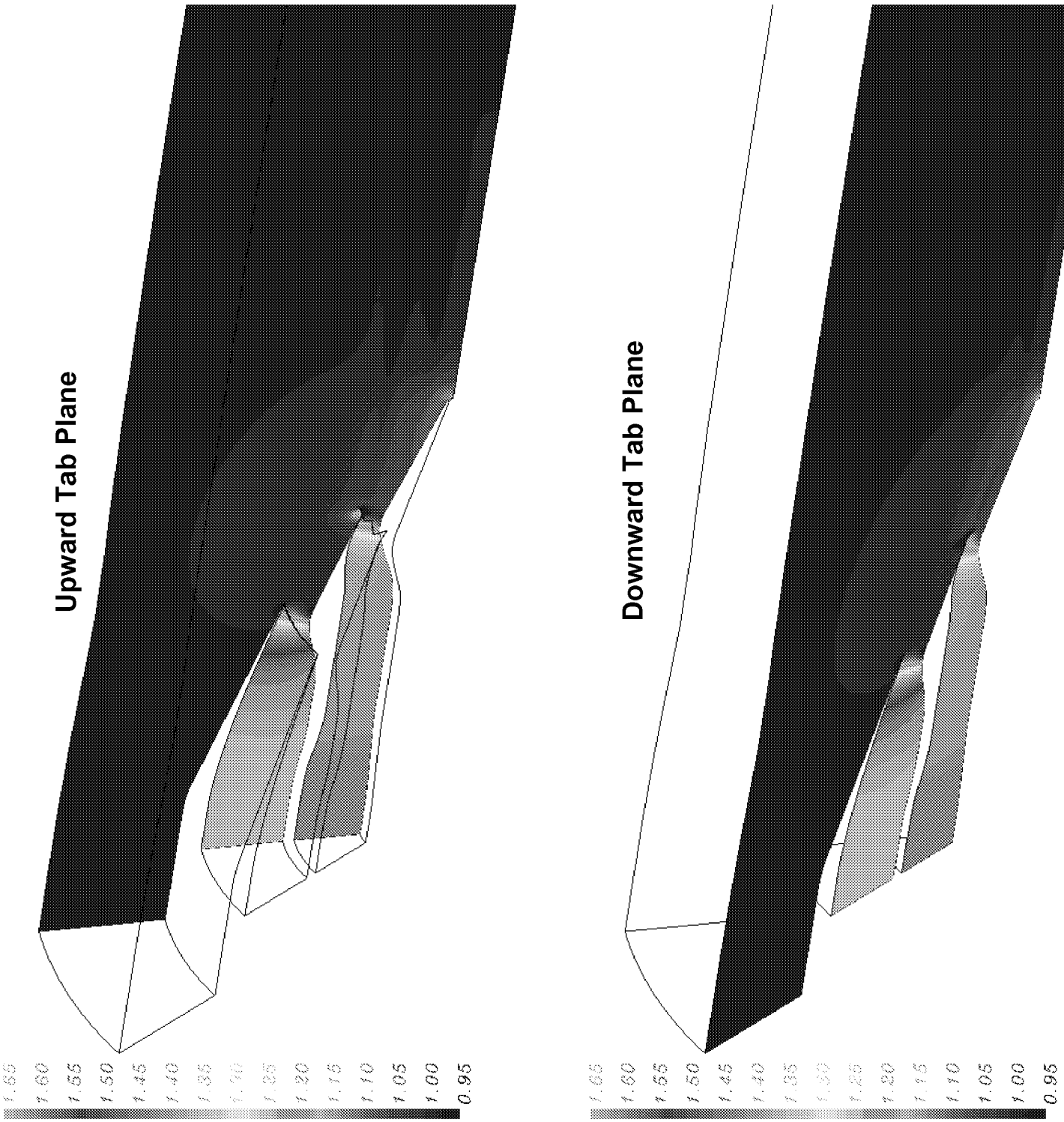
Upward Tab Plane
1.65
1.60
1.55
1.50
1.45
1.40
1.35
1.30
1.25
1.20
1.15
1.10
1.05
1.00
0.95
Downward Tab Plane
1.65
1.60
1.55
1.50
1.45
1.40
1.35
1.30
1.25
1.20
1.15
1.10
1.05
1.00
0.95

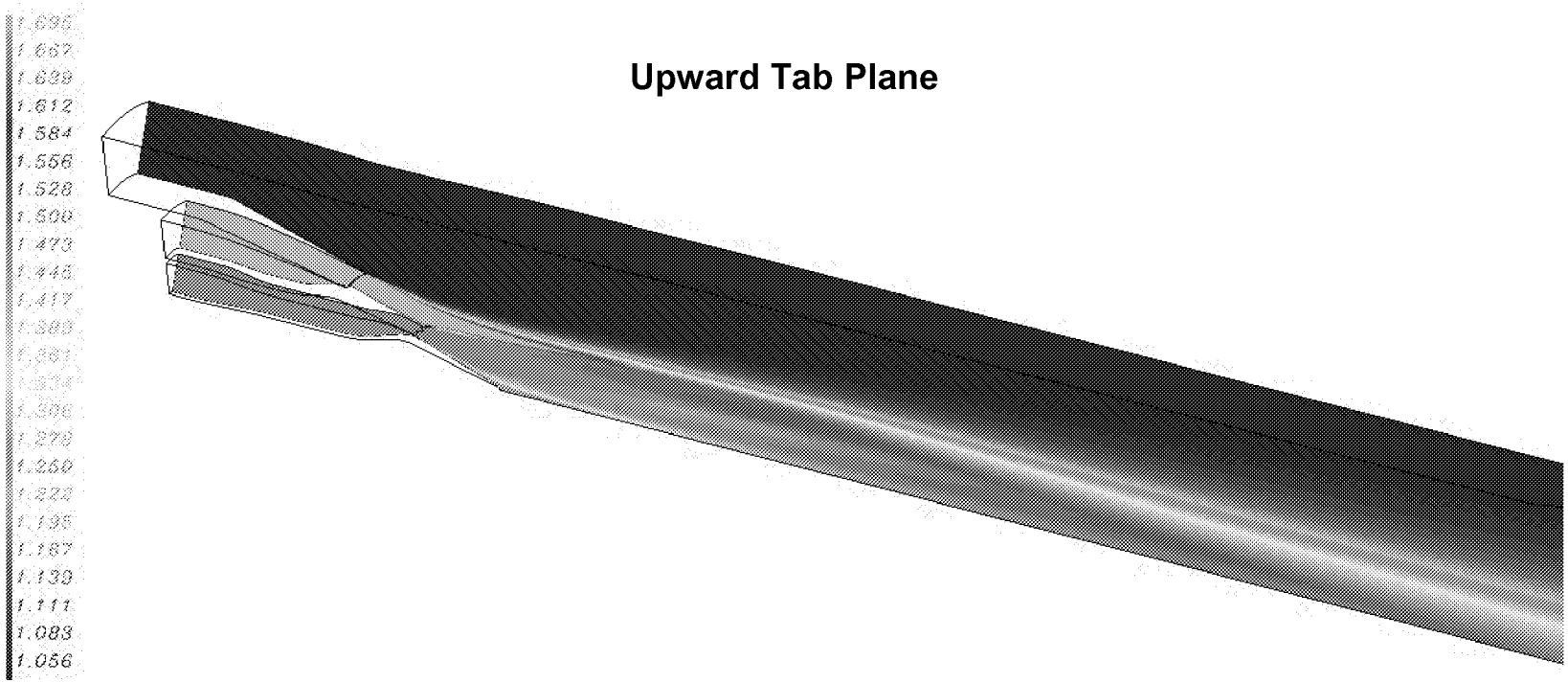

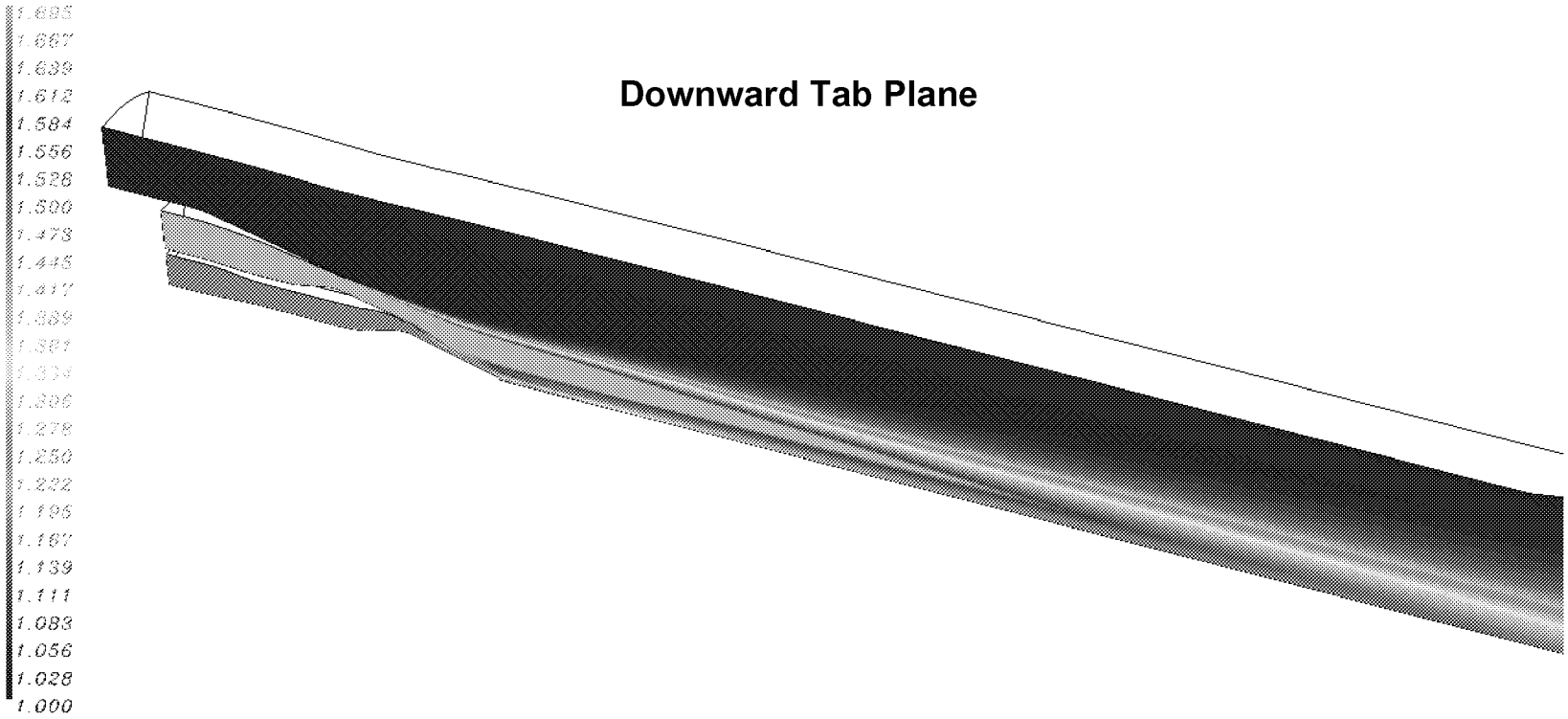

Figure 25. Stagnation pressure contours along symmetry planes for tab nozzle configuration.

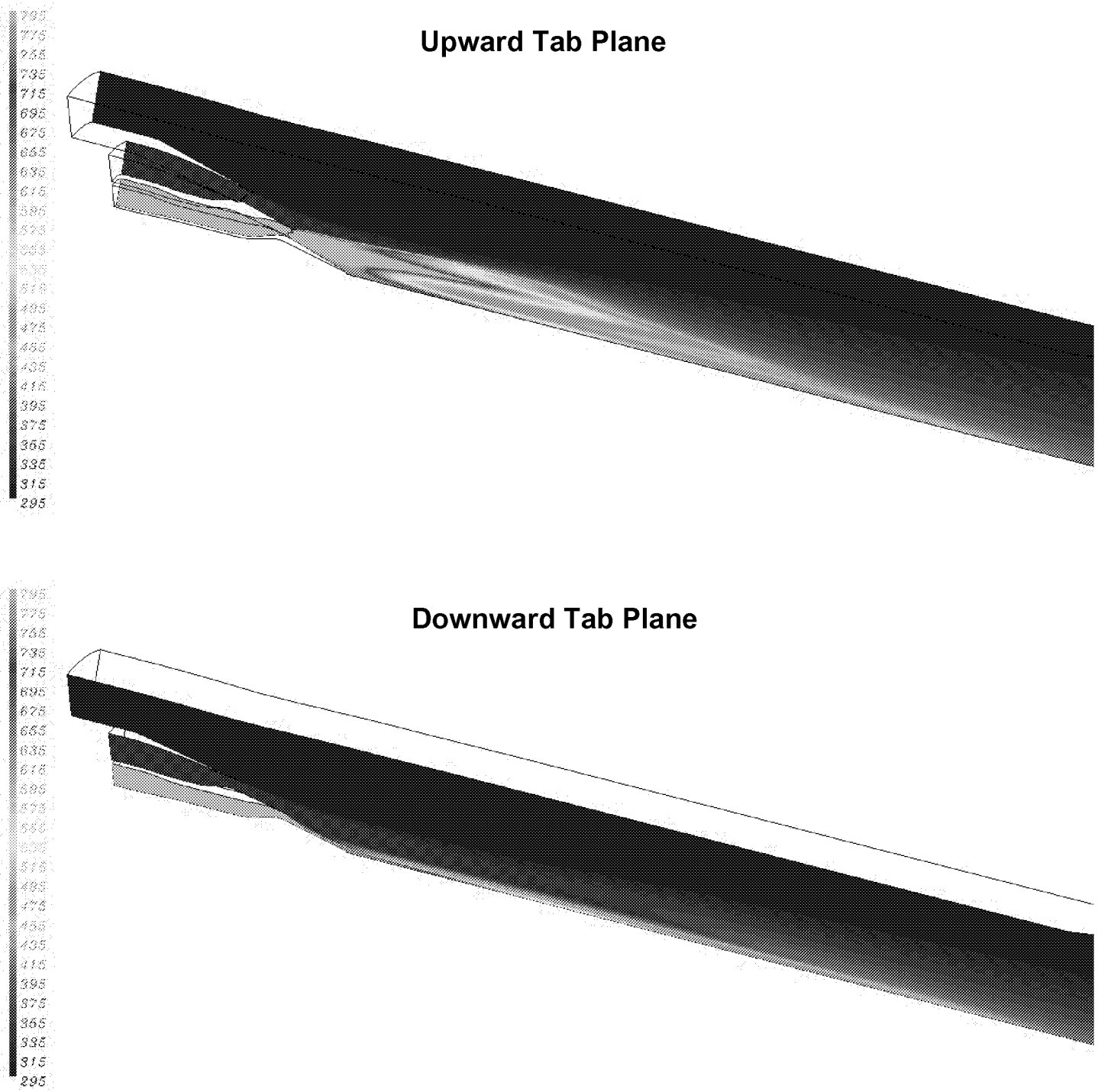

Figure 26. Total temperature contours along symmetry planes for tab nozzle configuration.

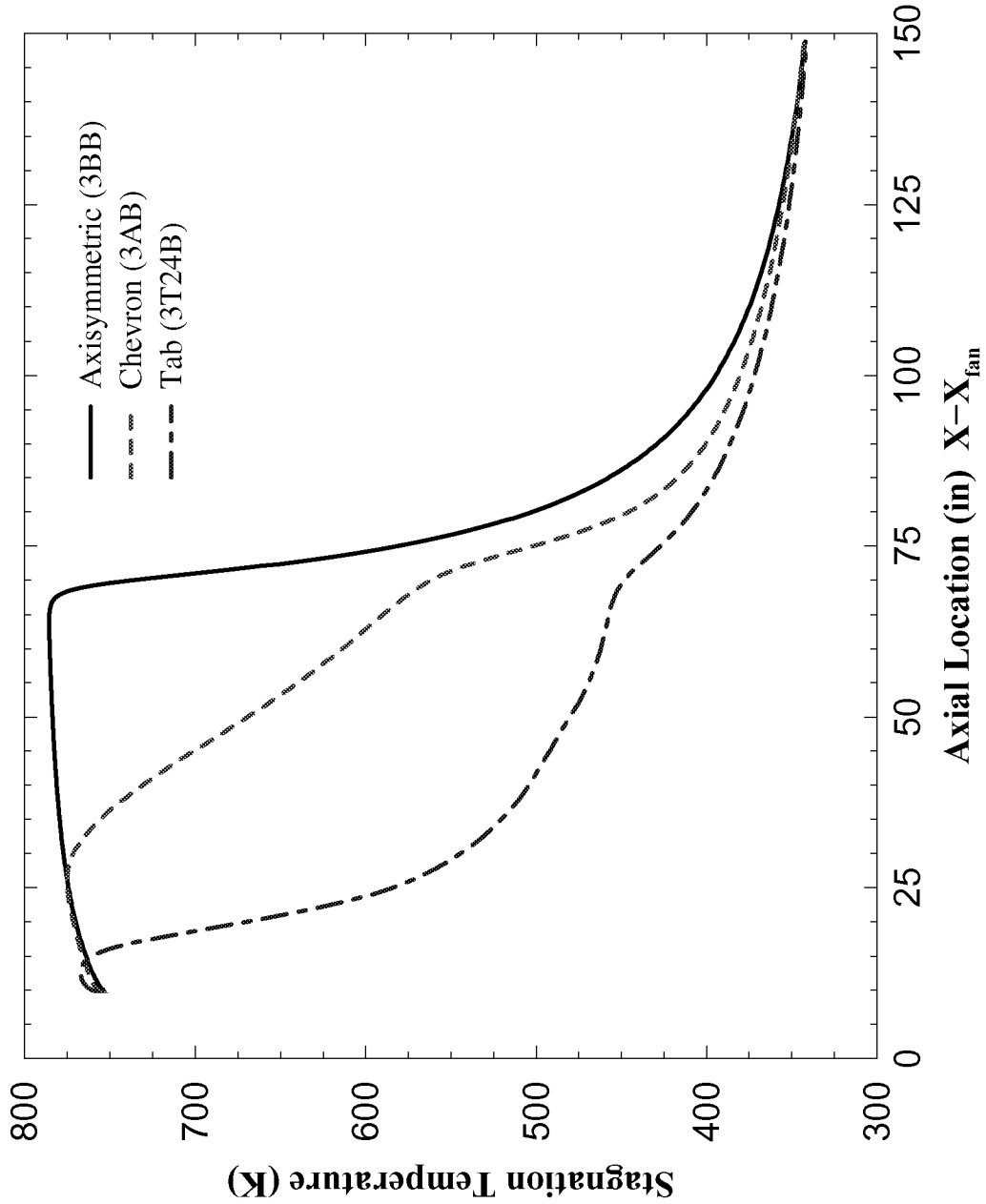

Figure 27. Comparison of total tempature decay along plume axis for nozzle configurations presently studied.

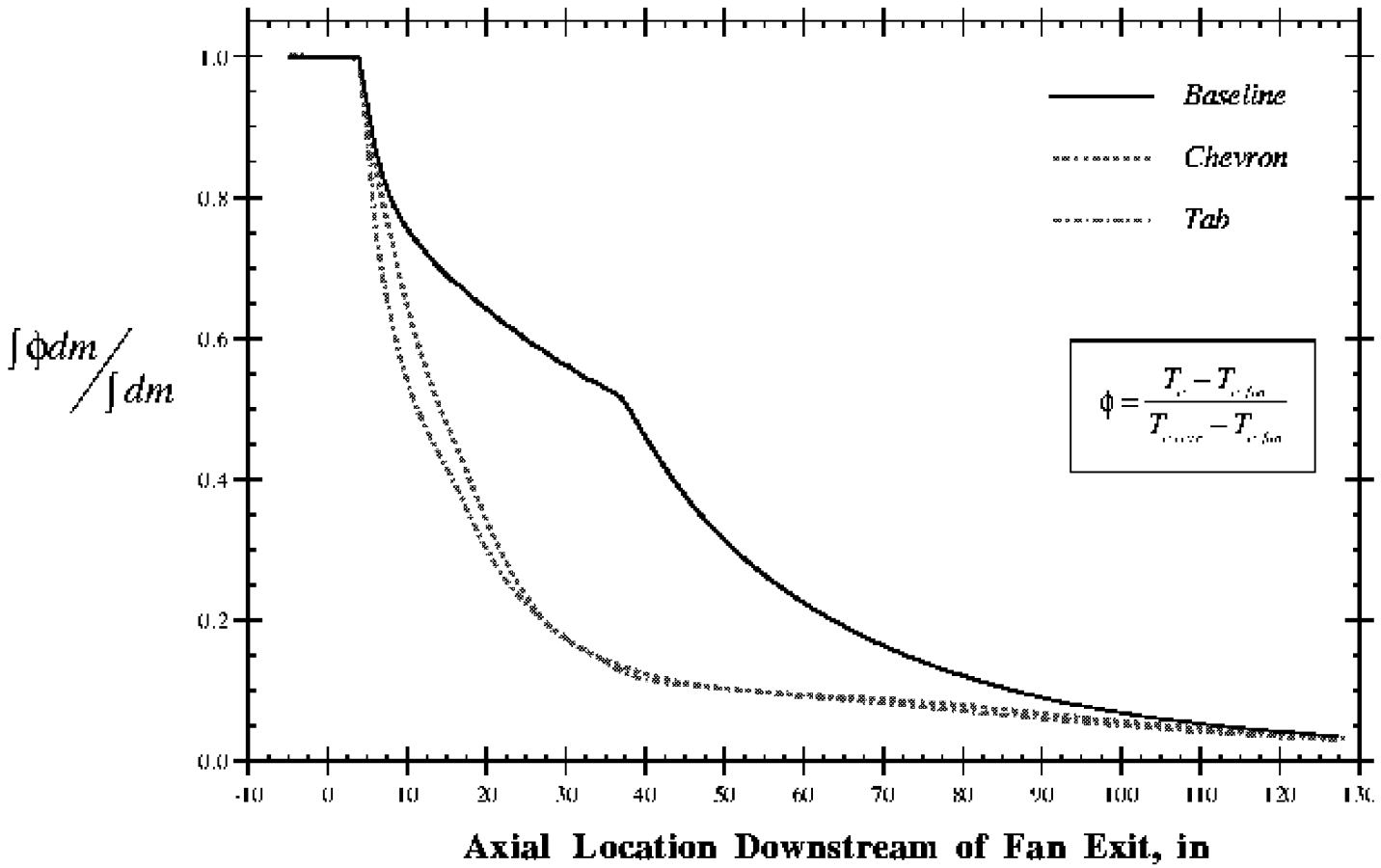

Figure 28. Stationwise integration of core stagnation temperature illustrating effects of passive mixing devices on plume mixing.

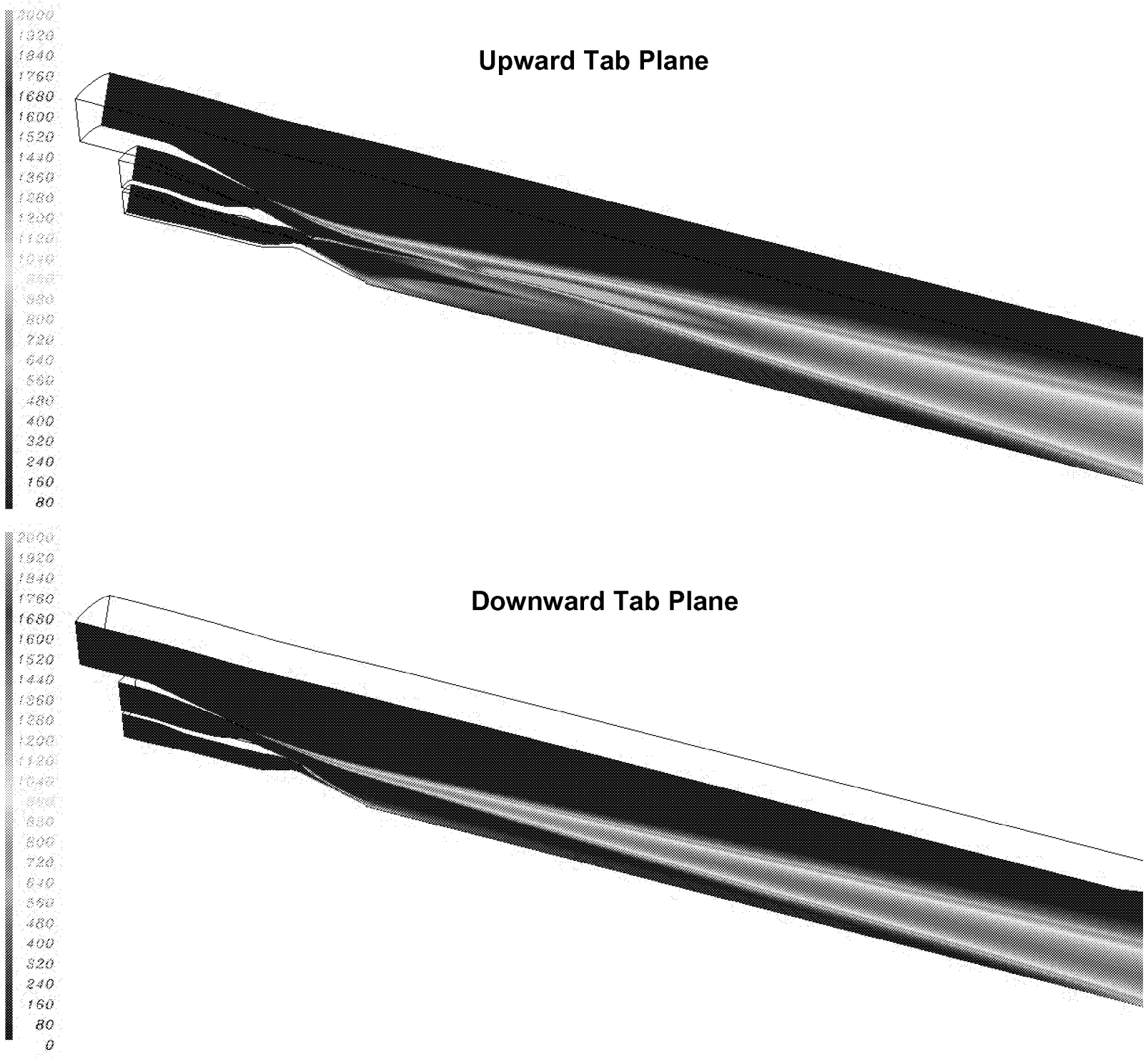

Figure 29. Turbulent kinetic energy contours along symmetry planes for tab nozzle configuration.

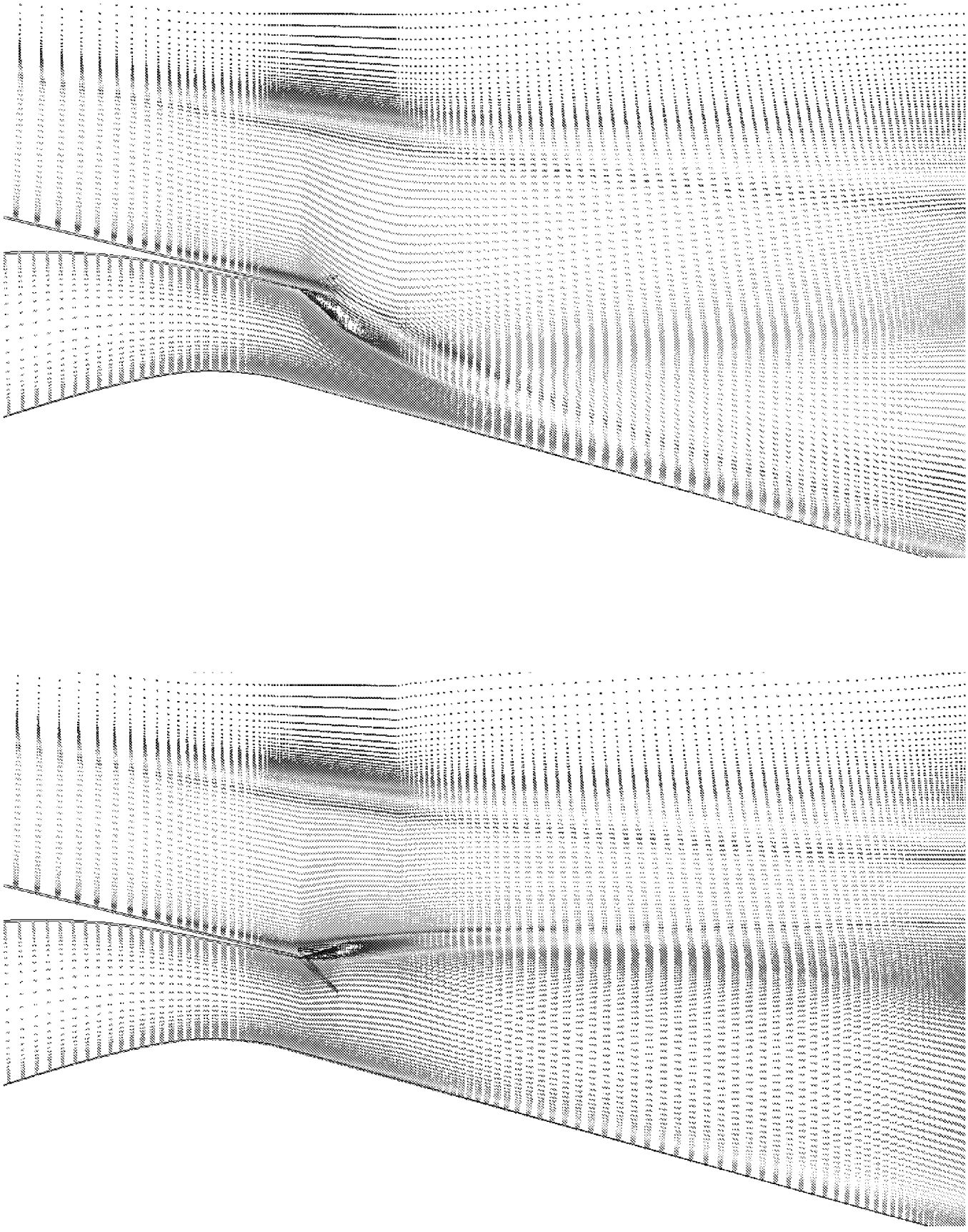

Figure 30. Velocity vectors colored by stagnation pressure indicating losses from recirculating regions.

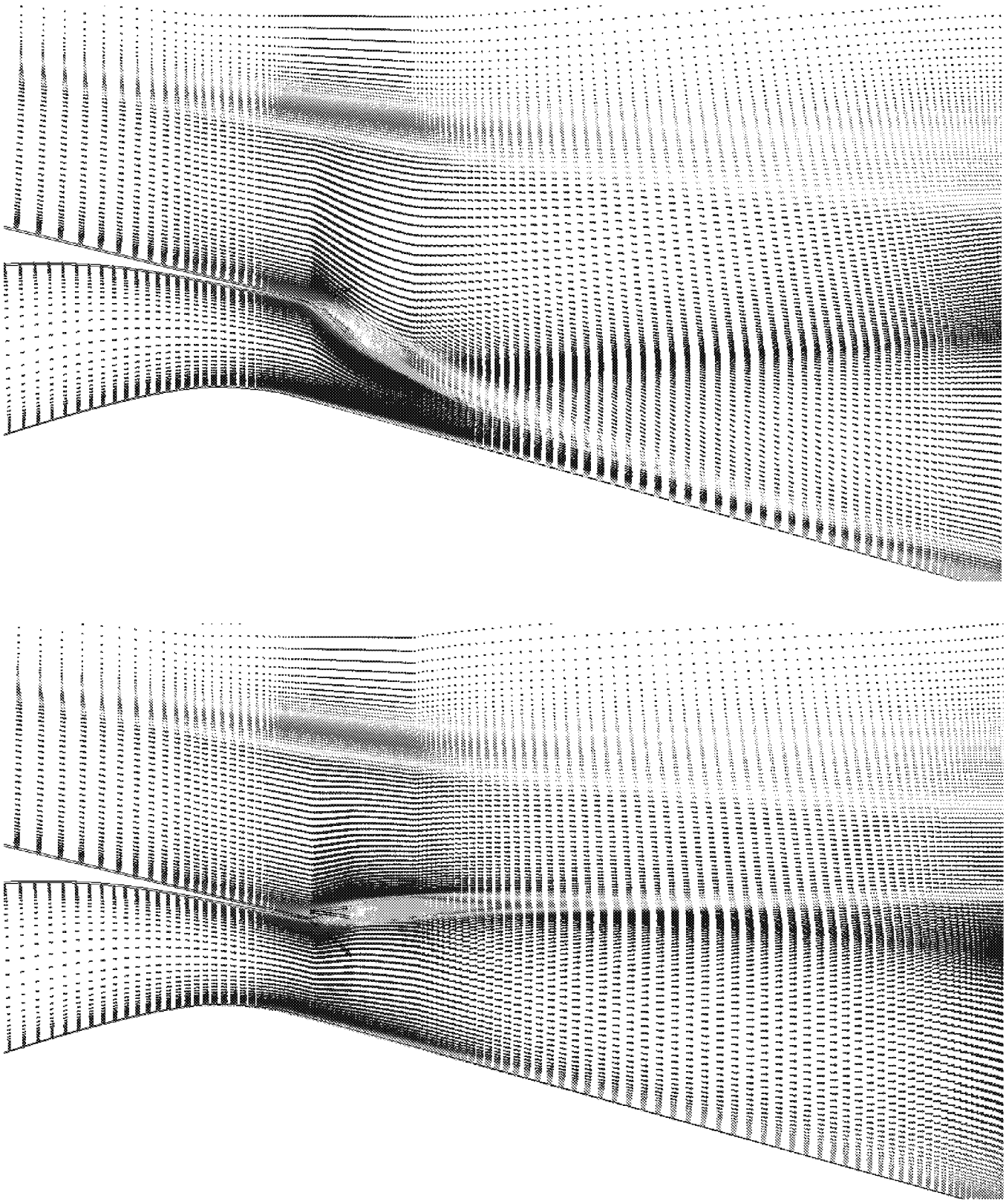

Figure 31. Velocity vectors colored by turbulent kinetic energy indicating peak values in recirculating regions.

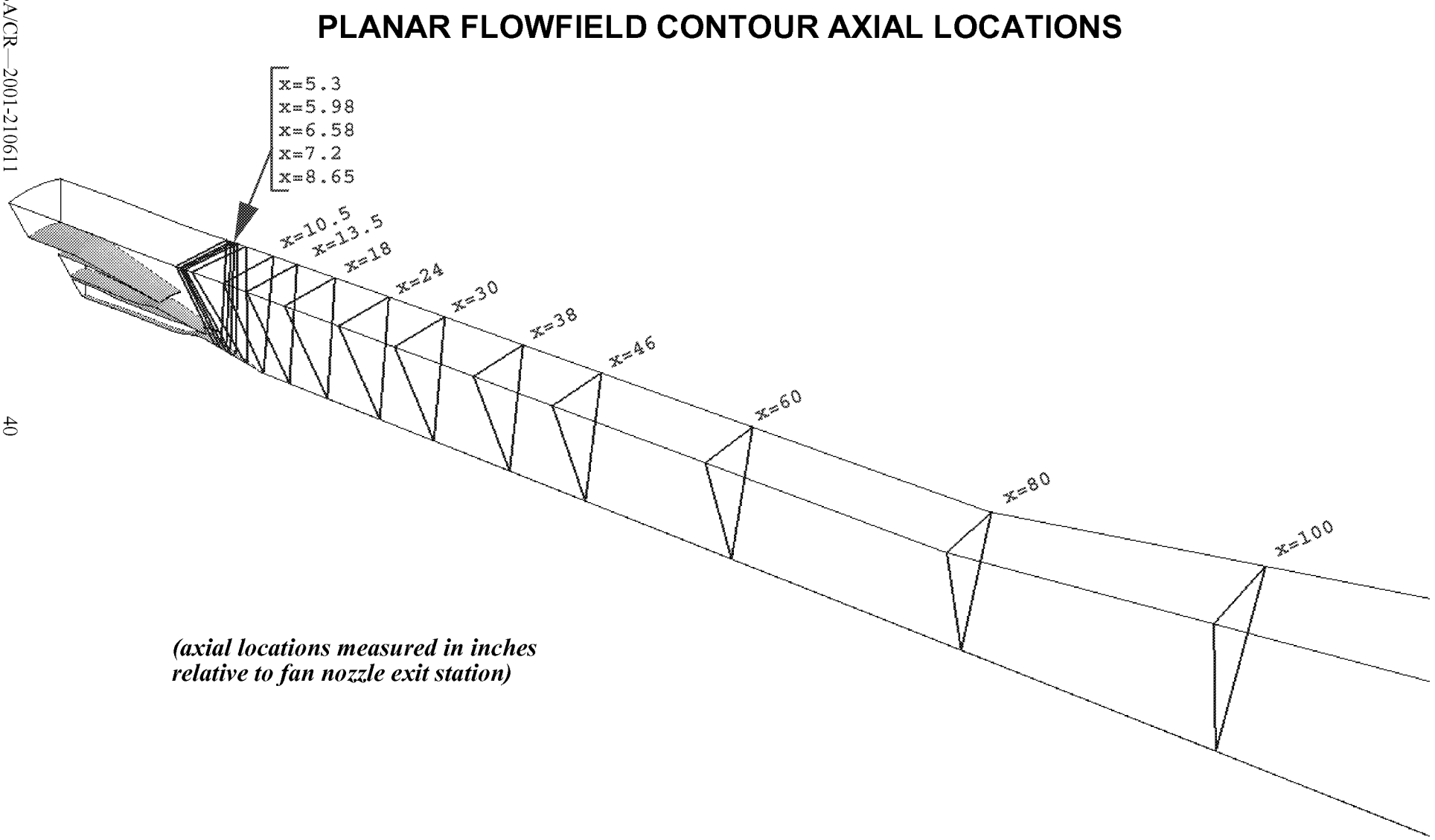

Figure 32. Axial station locations used for comparing baseline, chevron, and tab nozzle flowfields.

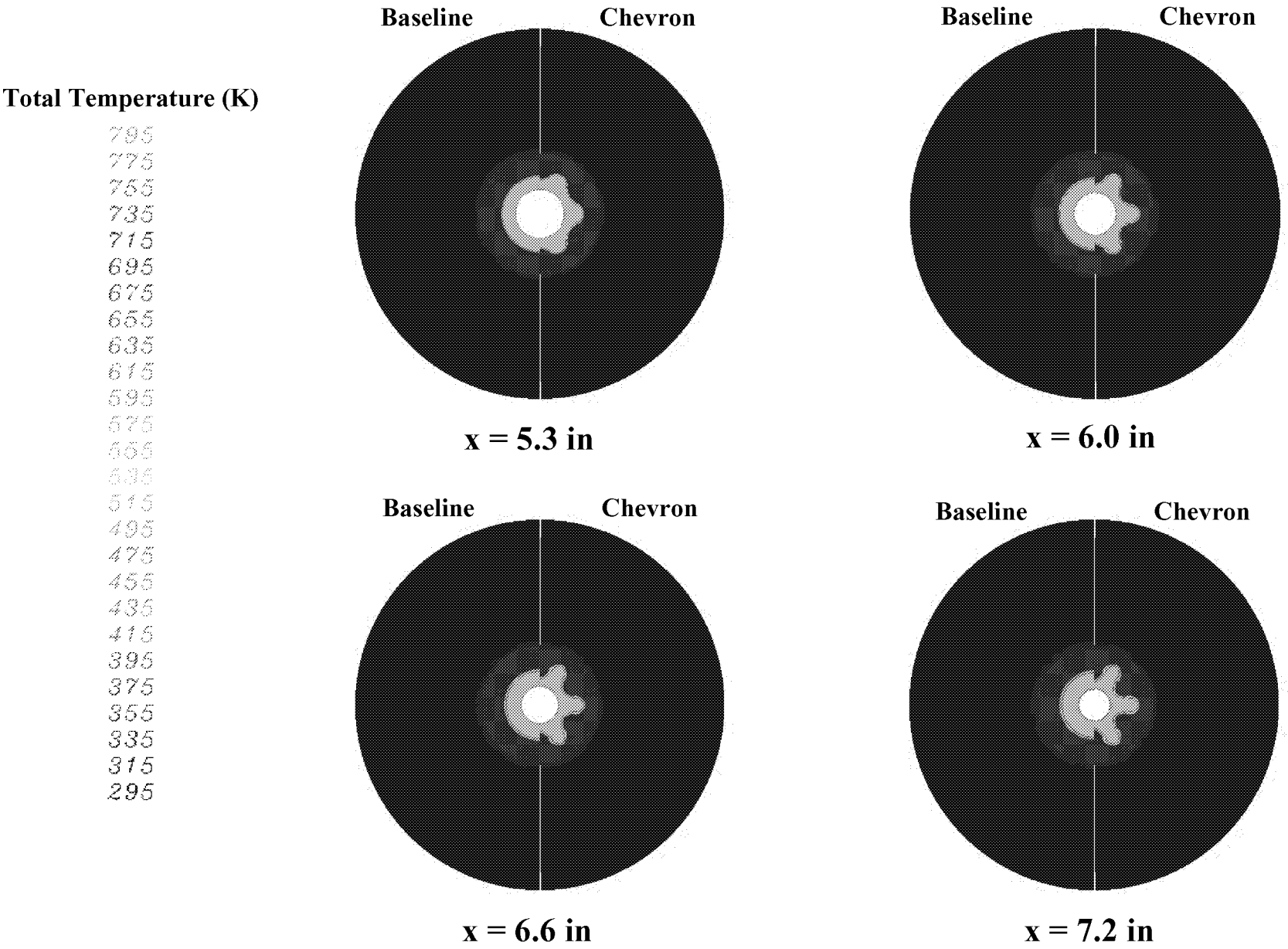

Figure 33. Comparison of total temperature contours for the axisymmetric and chevron flowfield solutions at selected axial atations.

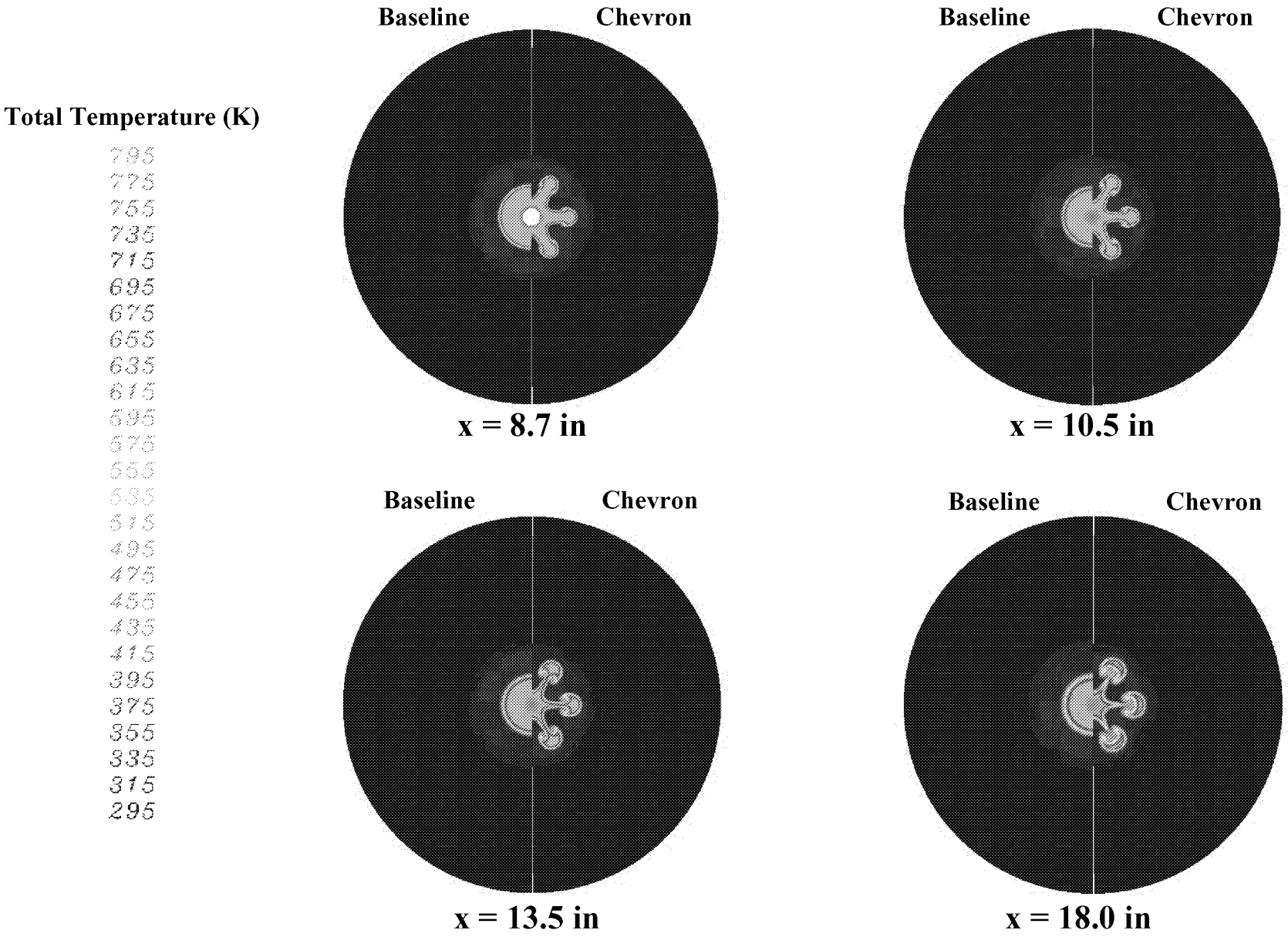

Figure 33. Comparison of total temperature contours (cont'd).

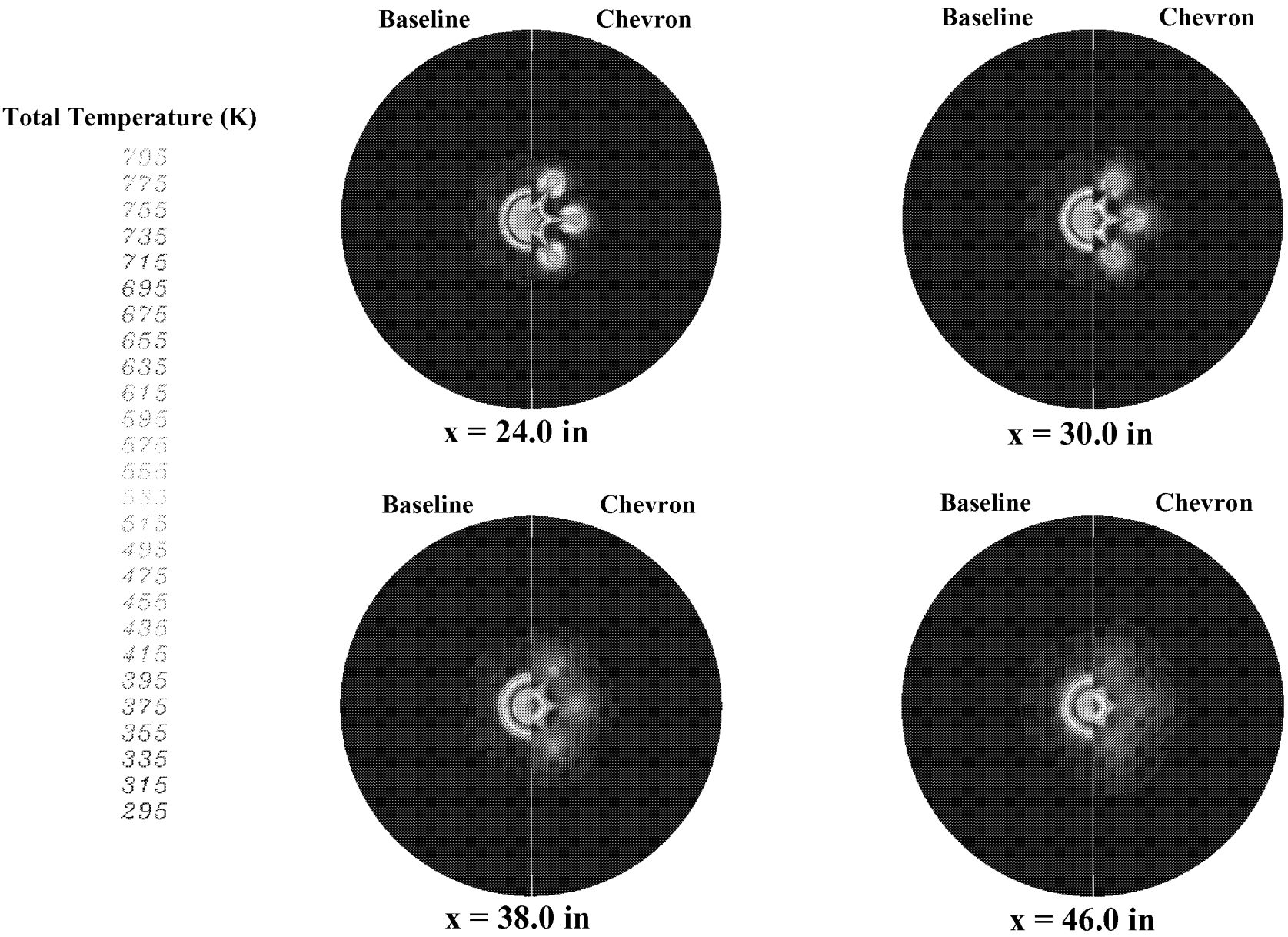

Figure 33. Comparison of total temperature contours (cont'd).

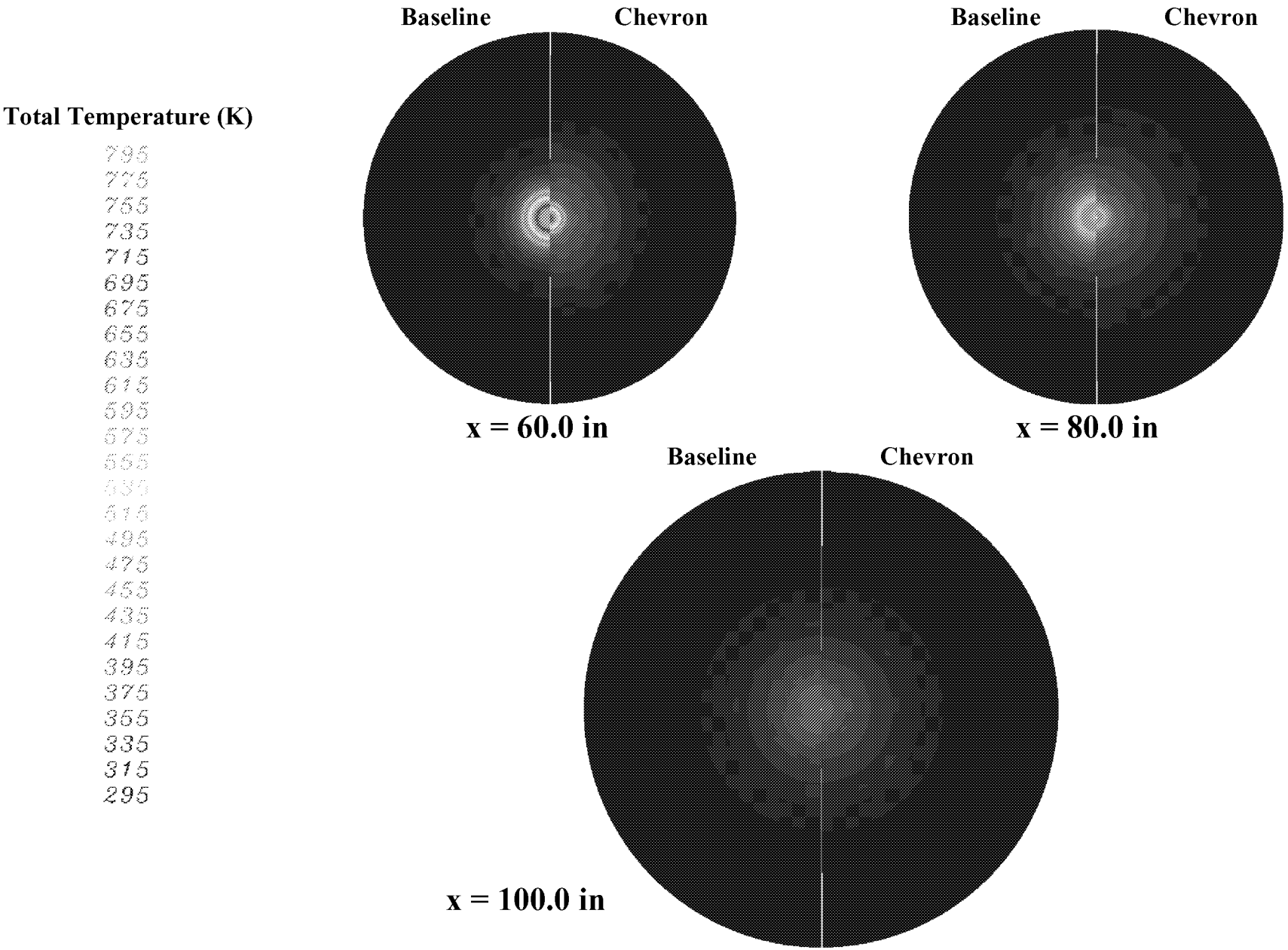

Figure 33. Comparison of total temperature contours (cont'd).

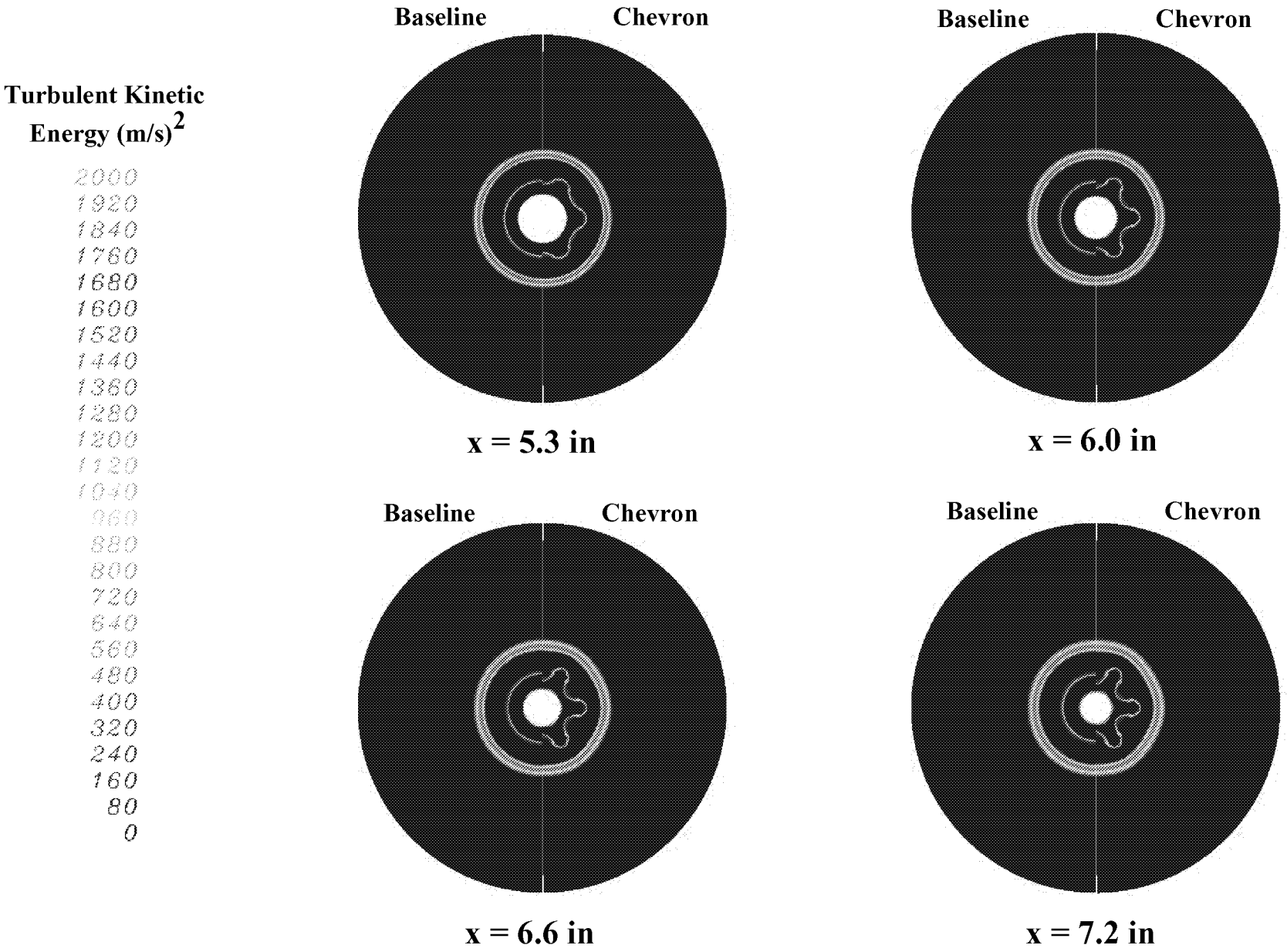

Figure 34. Comparison of turbulent kinetic energy contours for the chevron and tab flowfield solutions at selected axial atations.

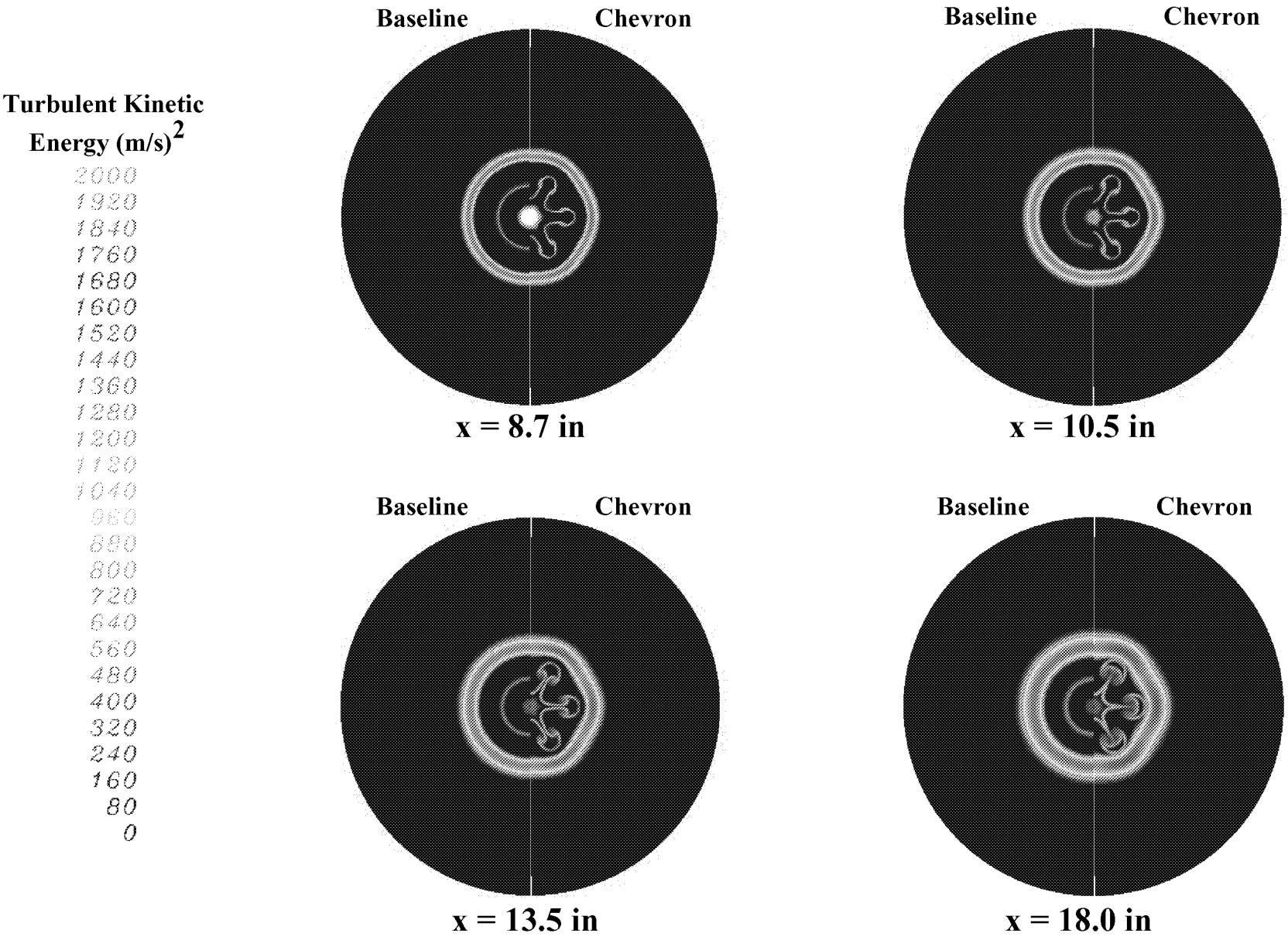

Figure 34. Comparison ofturbulent kinetic energy contours (cont'd).

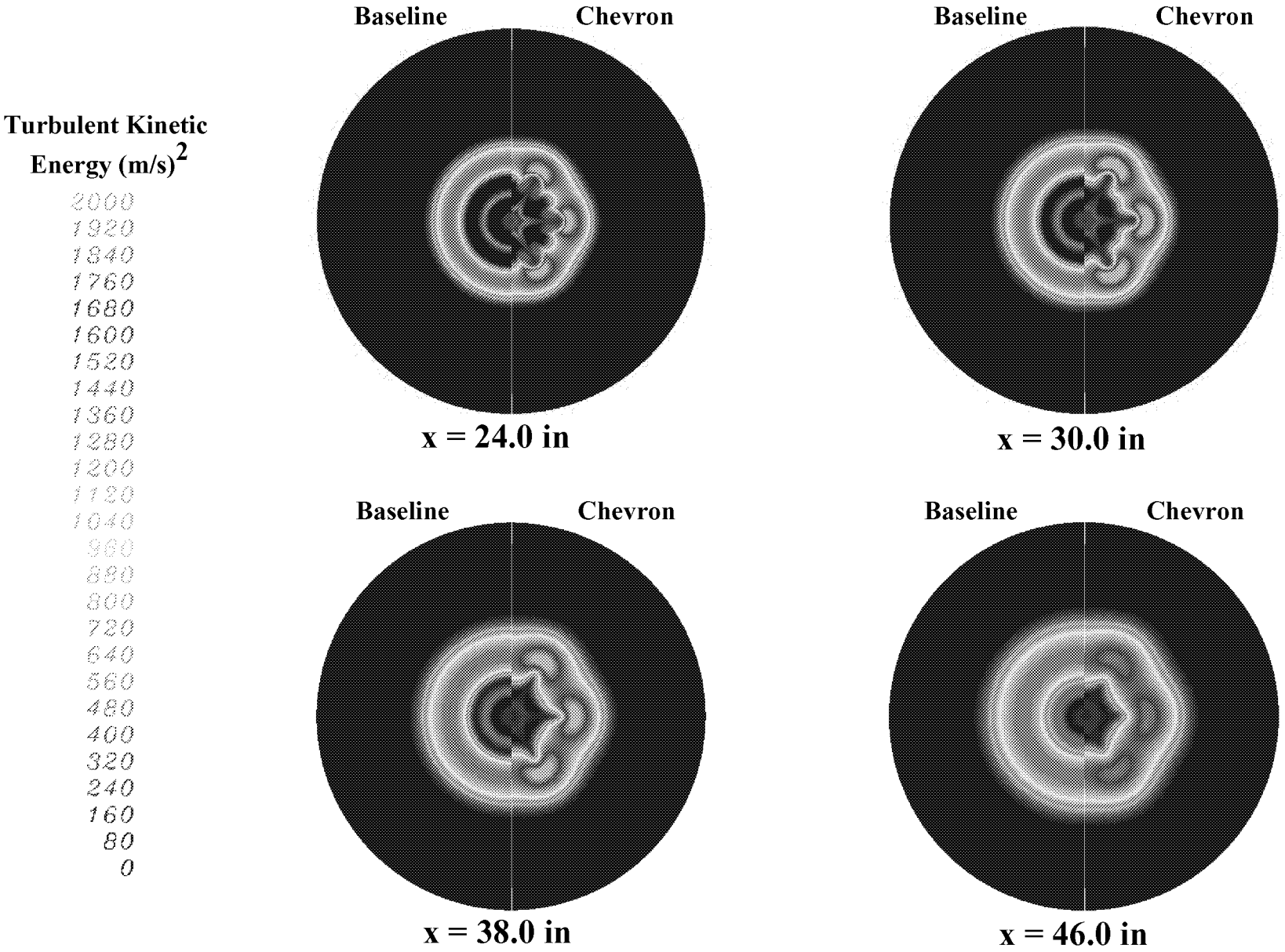

Figure 34. Comparison ofturbulent kinetic energy contours (cont'd).

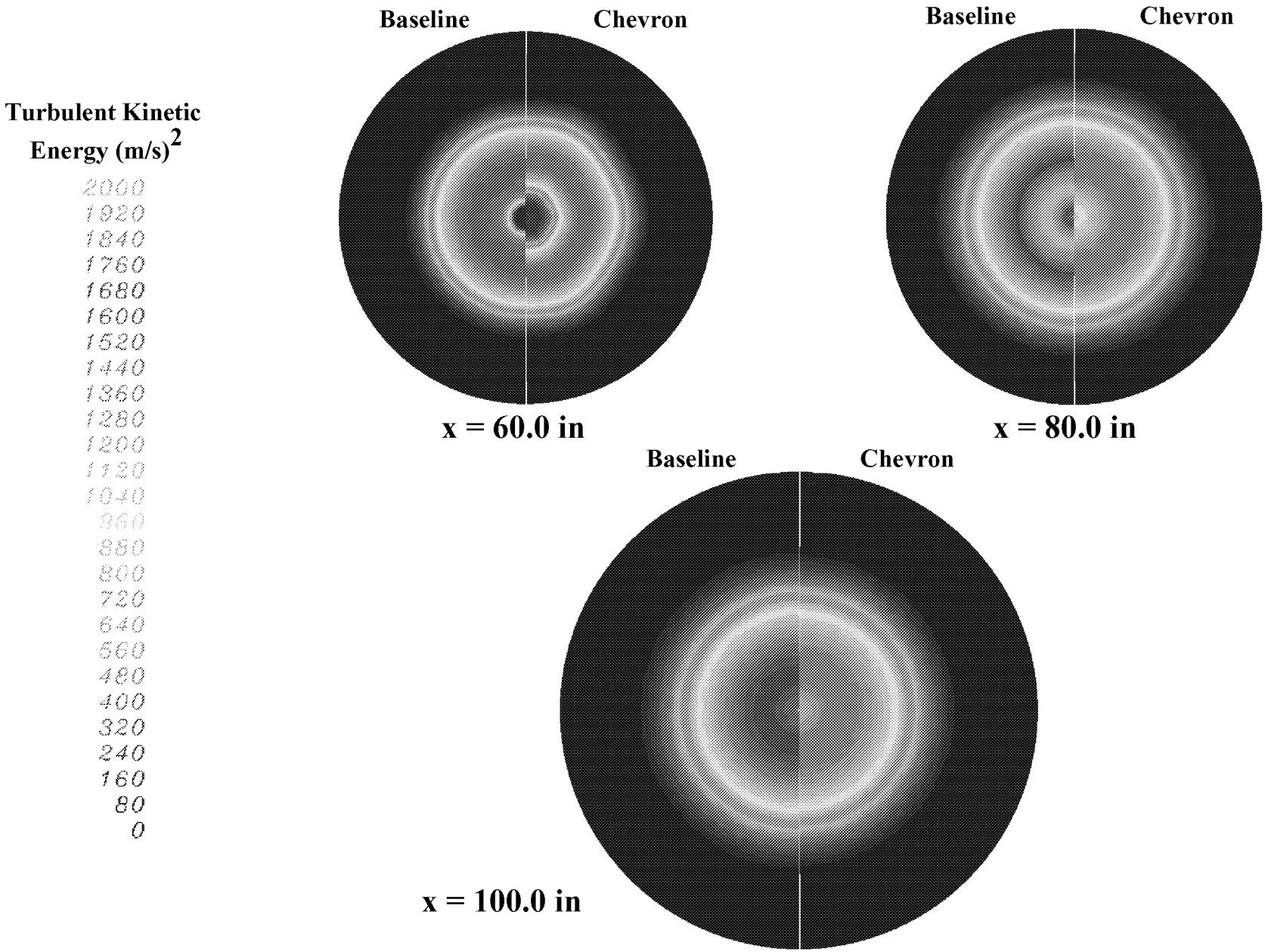

Figure 34. Comparison ofturbulent kinetic energy contours (cont'd).

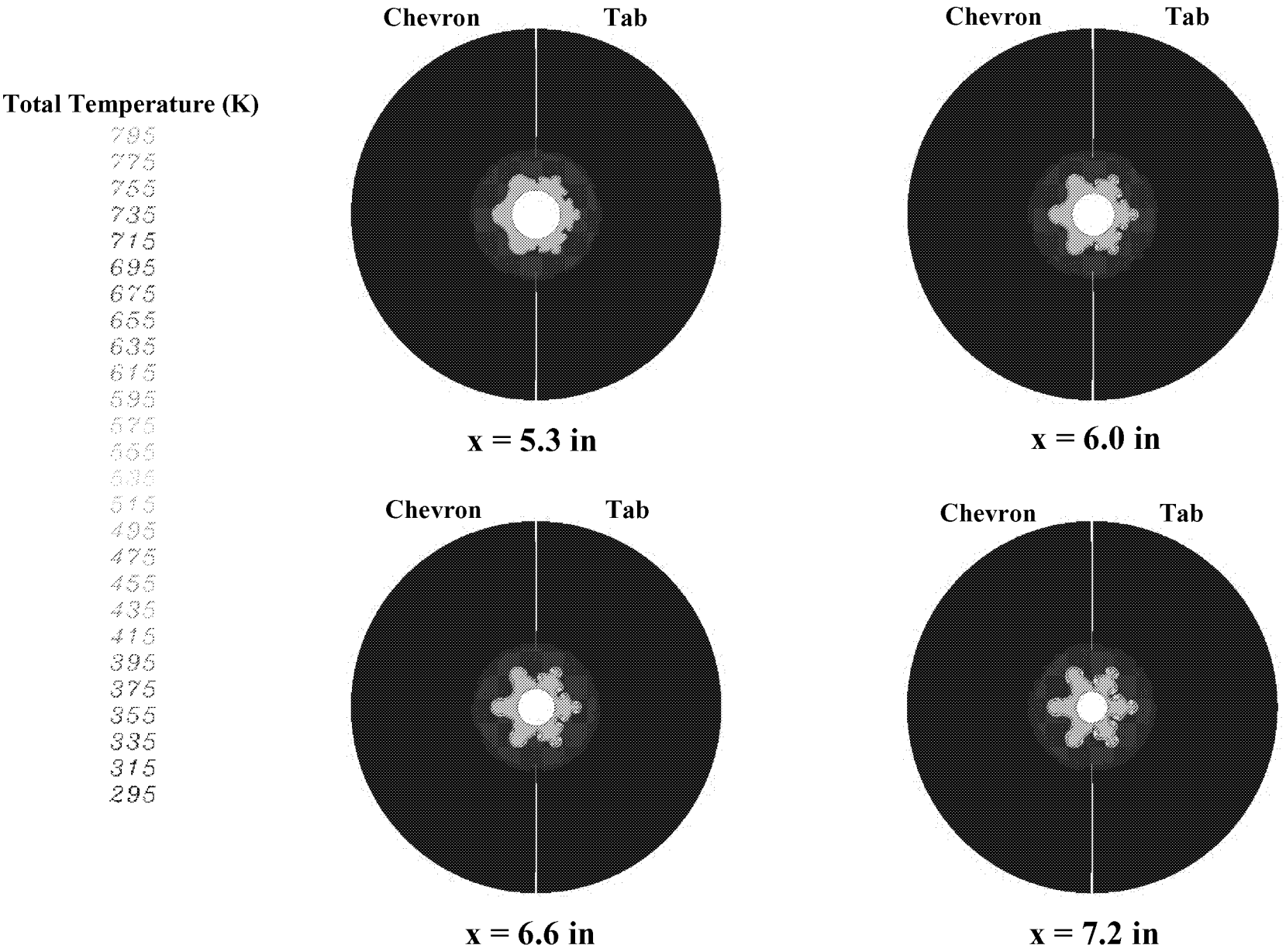

Figure 35. Comparison of total temperature contours for the chevron and tab flowfield solutions at selected axial atations.

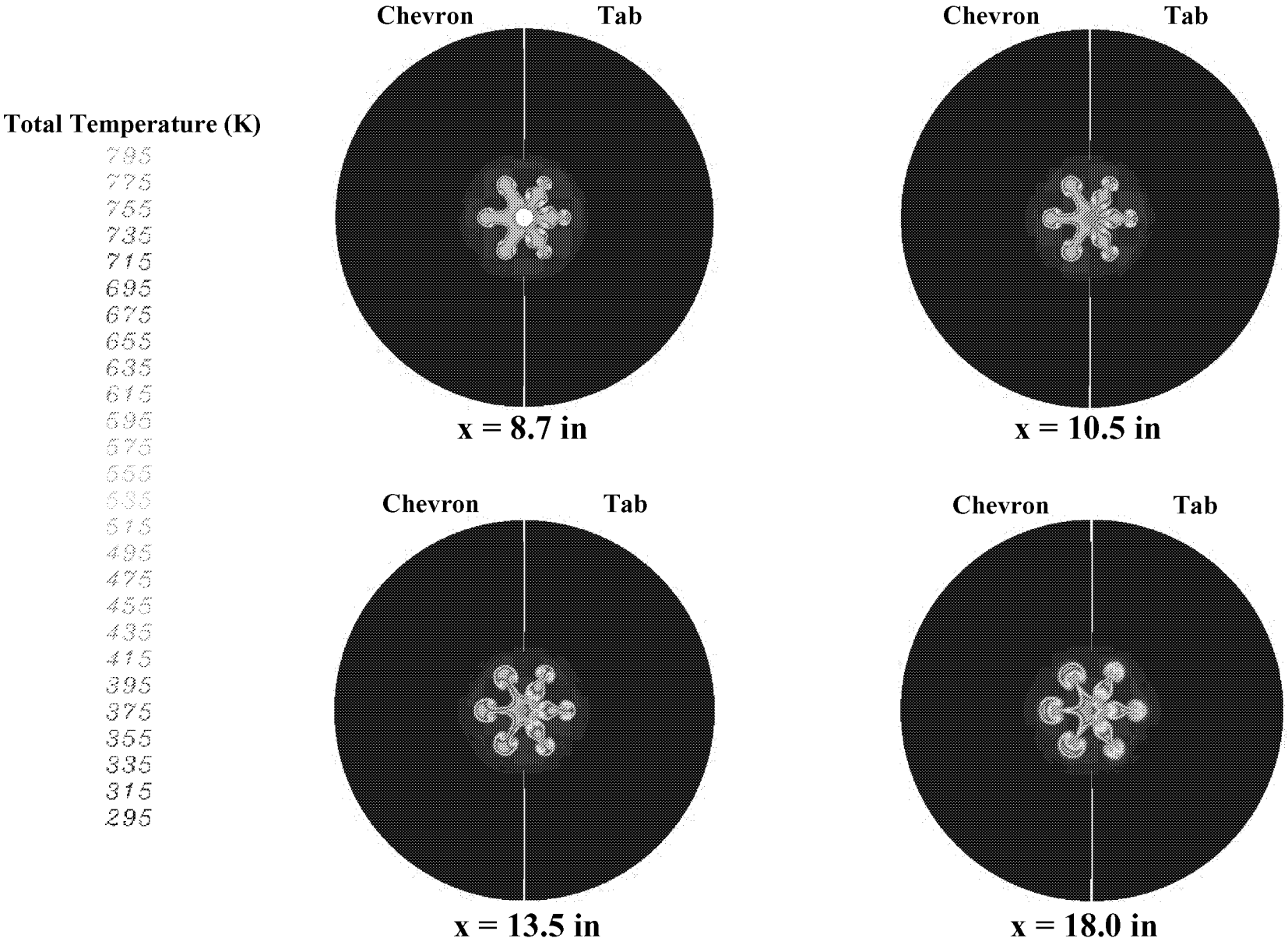

Figure 35. Comparison of total temperature contours (continued).

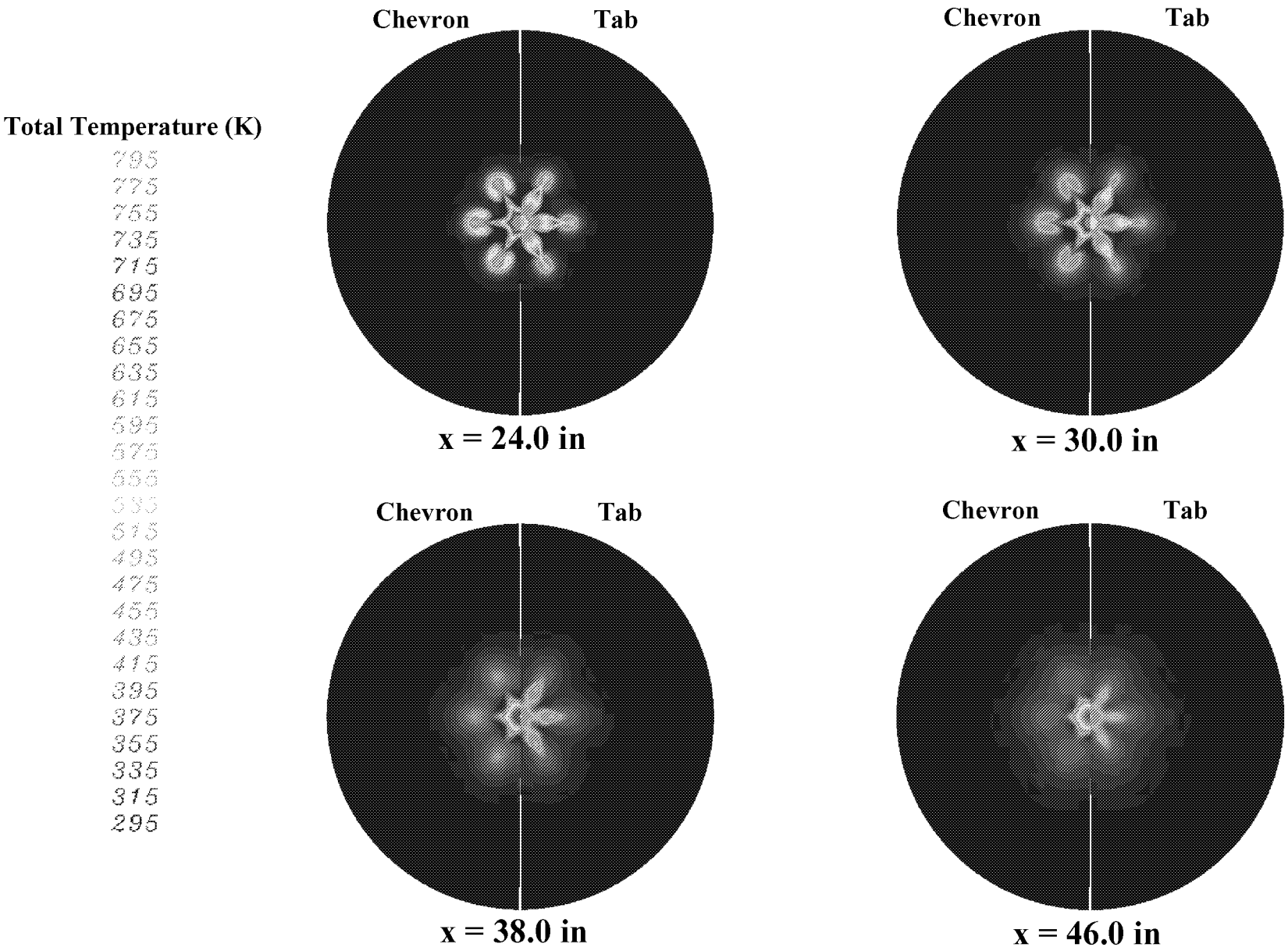

Figure 35. Comparison of total temperature contours (continued).

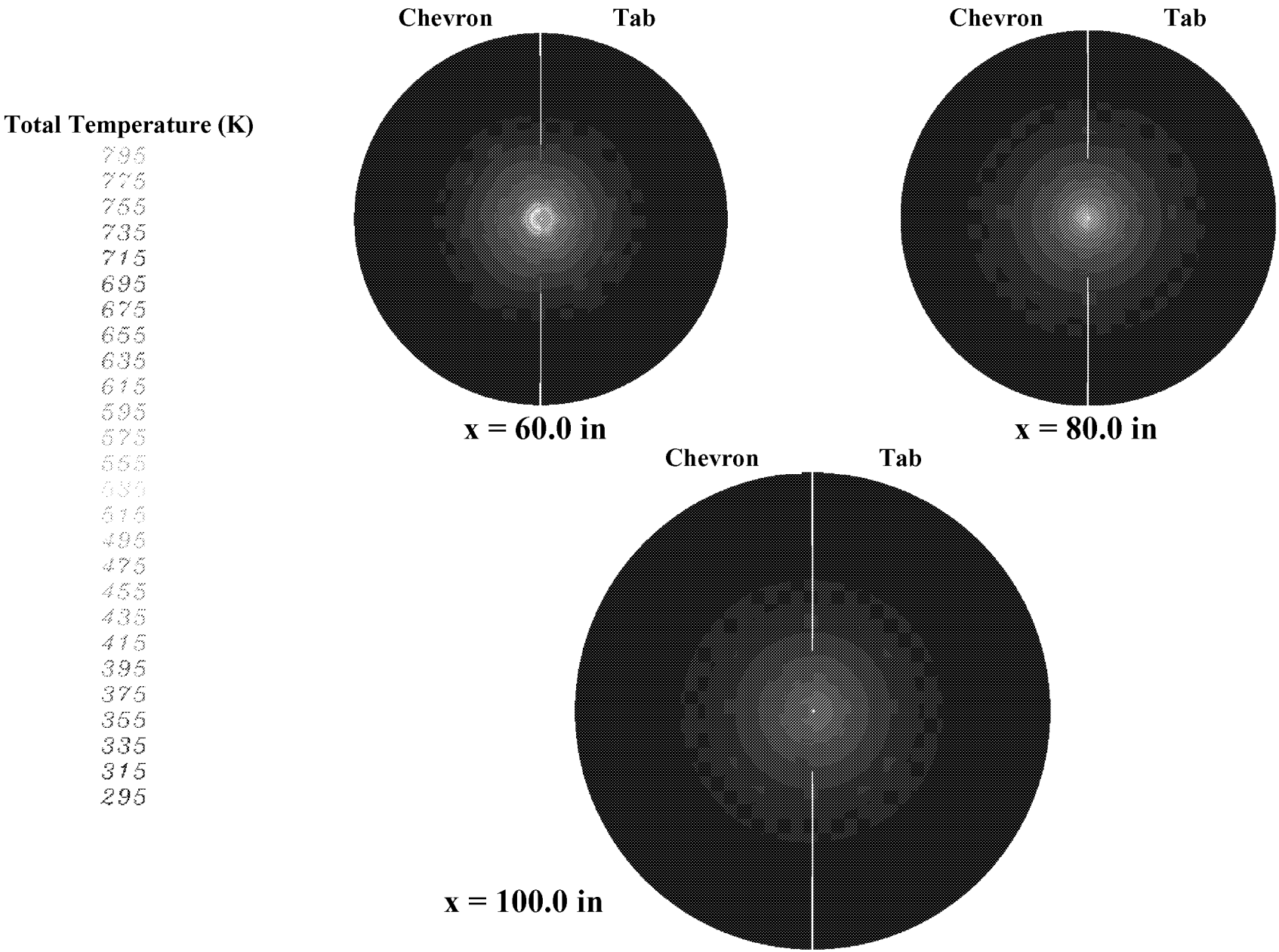

Figure 35. Comparison of total temperature contours (continued).

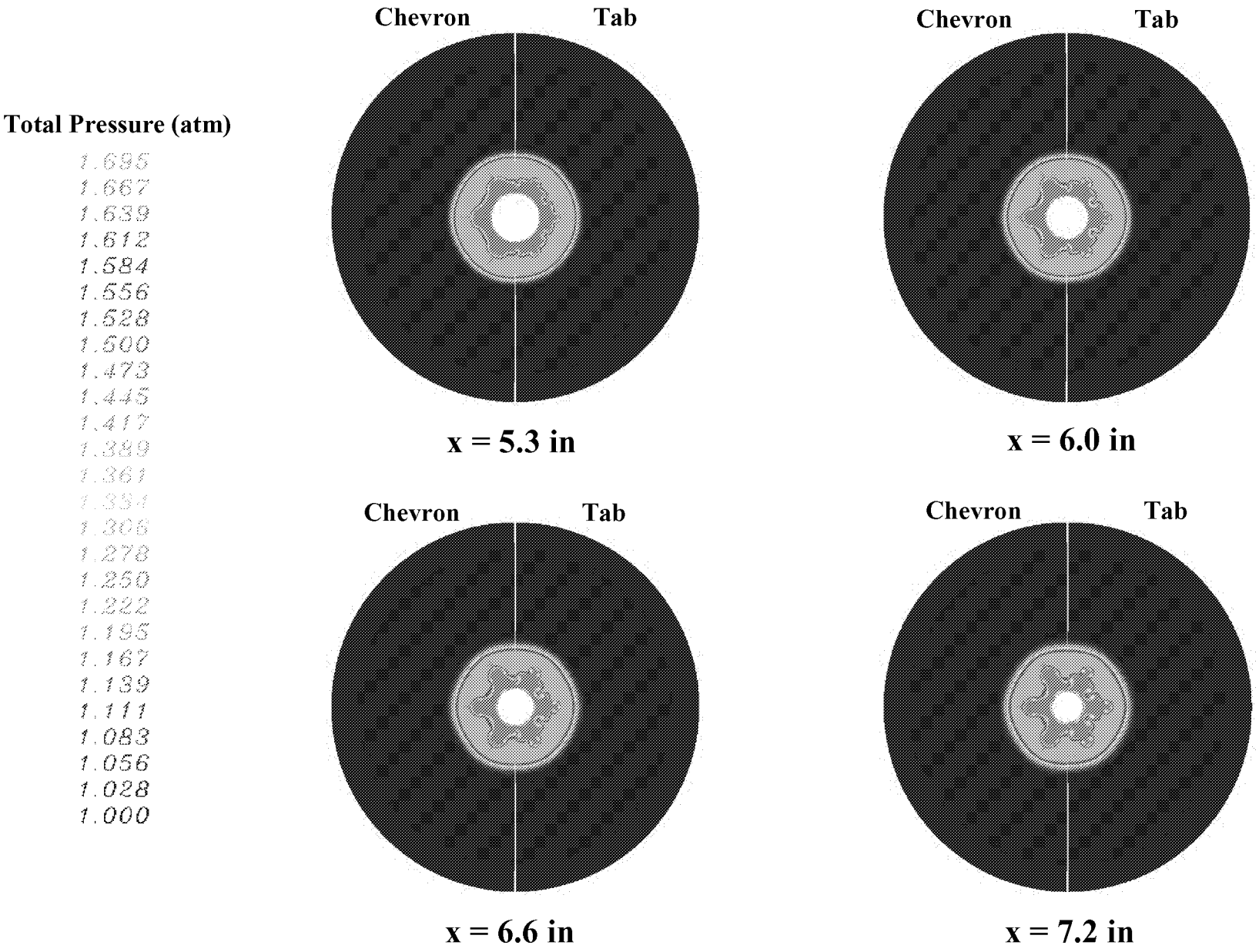

Figure 36. Comparison of stagnation pressure contours for the chevron and tab nozzle configurations at selected stations.

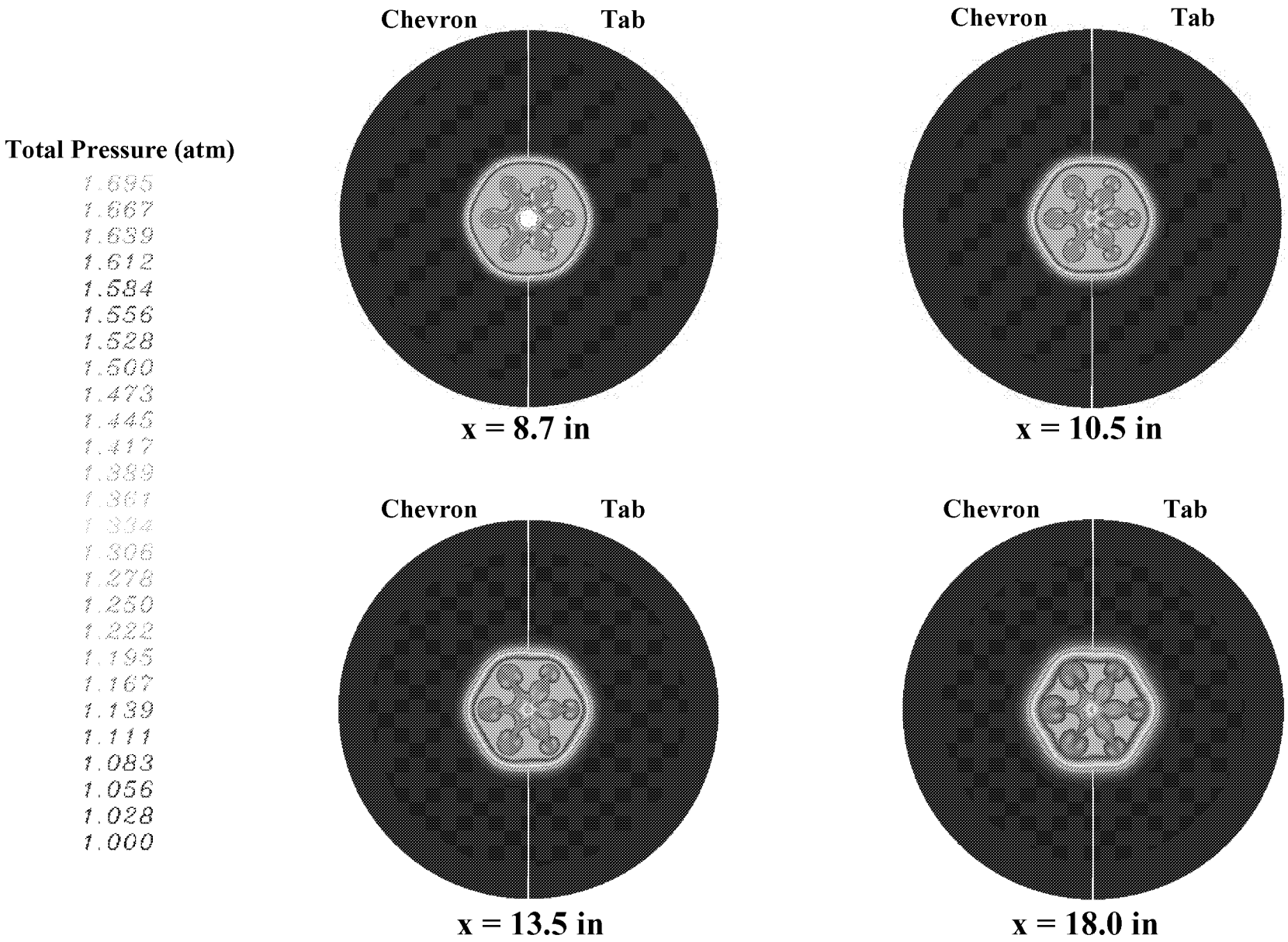

Figure 36. Comparison of stagnation pressure contours (continued).

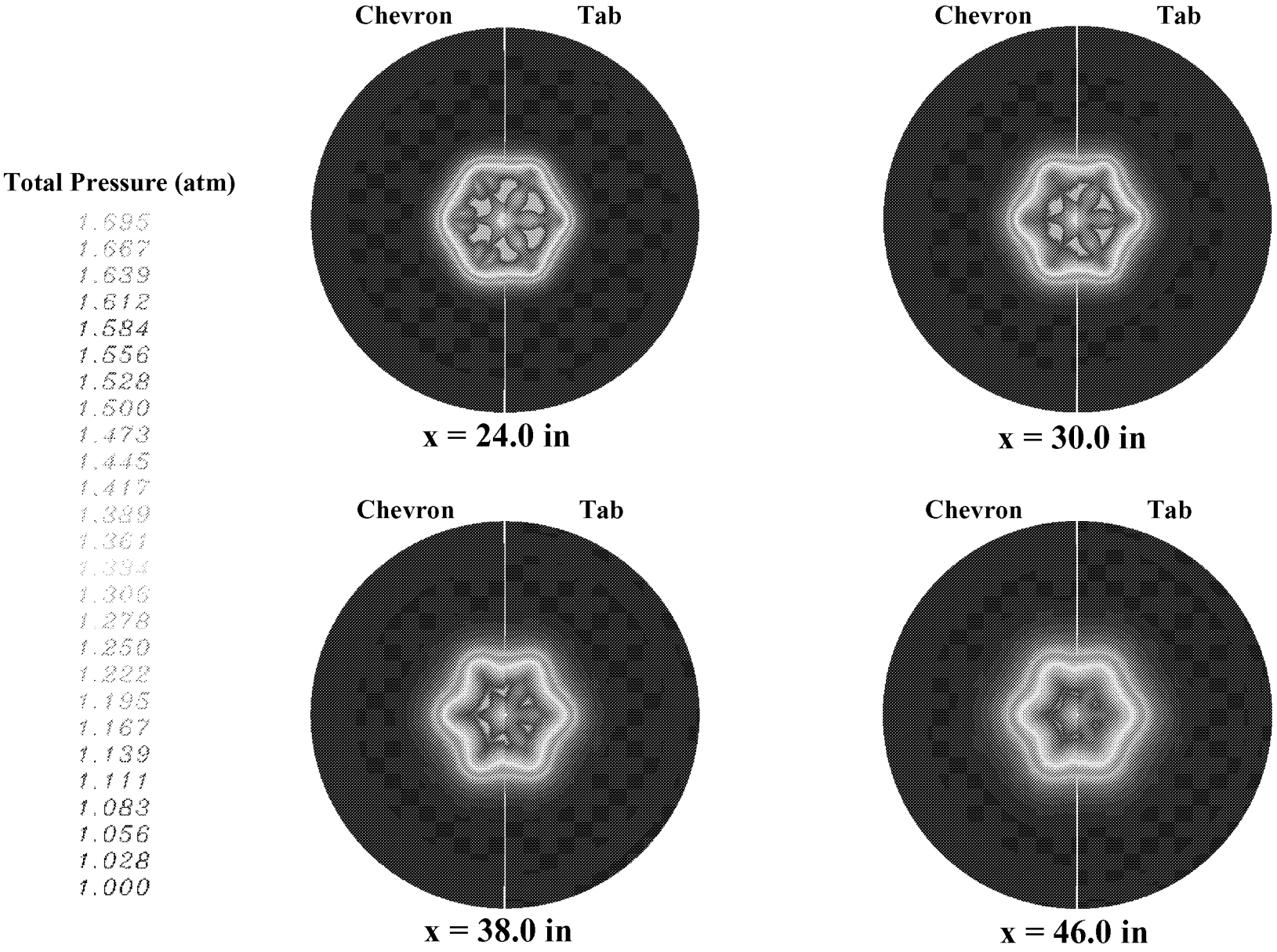

Figure 36. Comparison of stagnation pressure contours (continued).

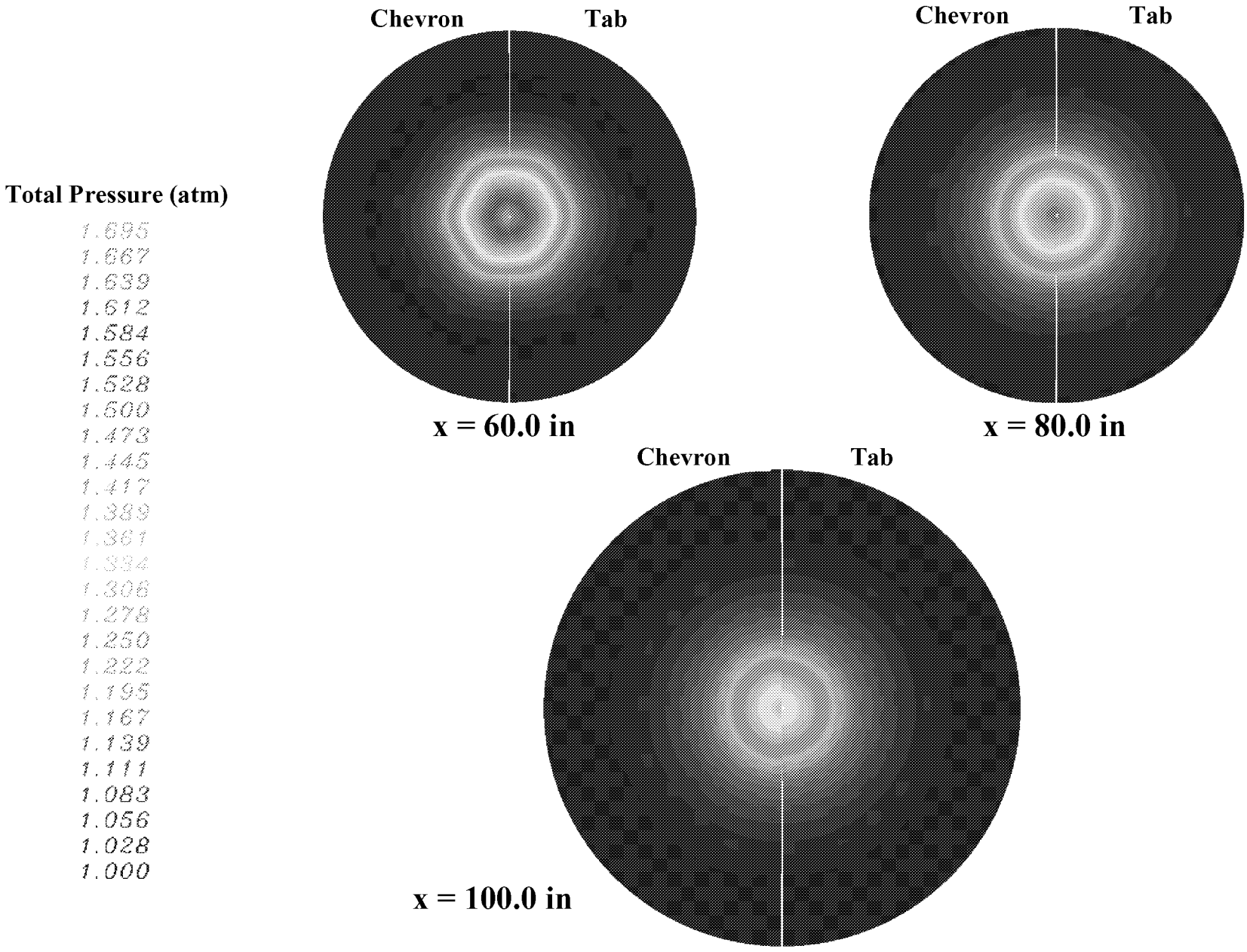

Figure 36. Comparison of stagnation pressure contours (continued).

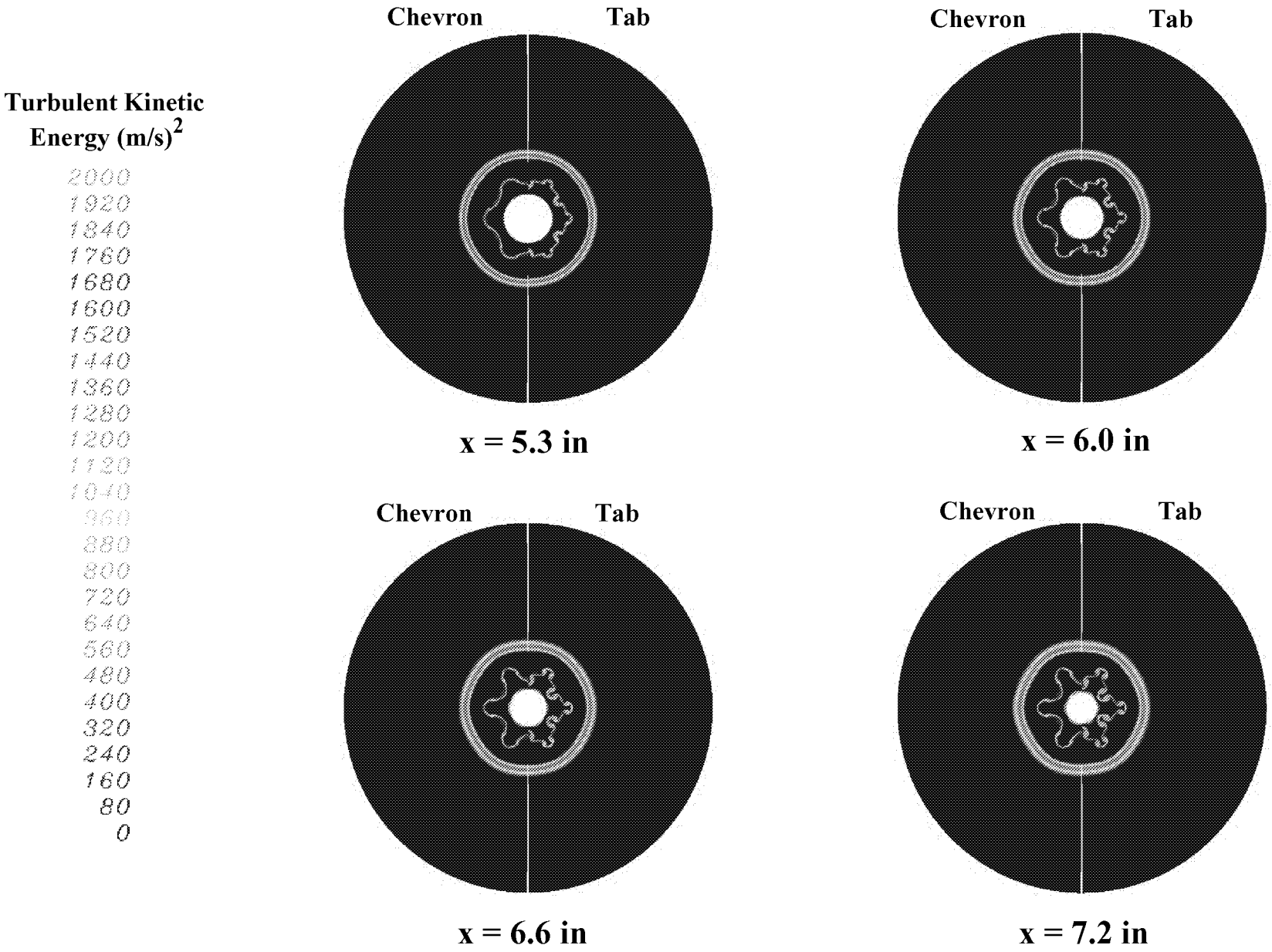

Figure 37. Comparison of turbulent kinetic energy contours for the chevron and tab nozzle flowfields at selected stations..

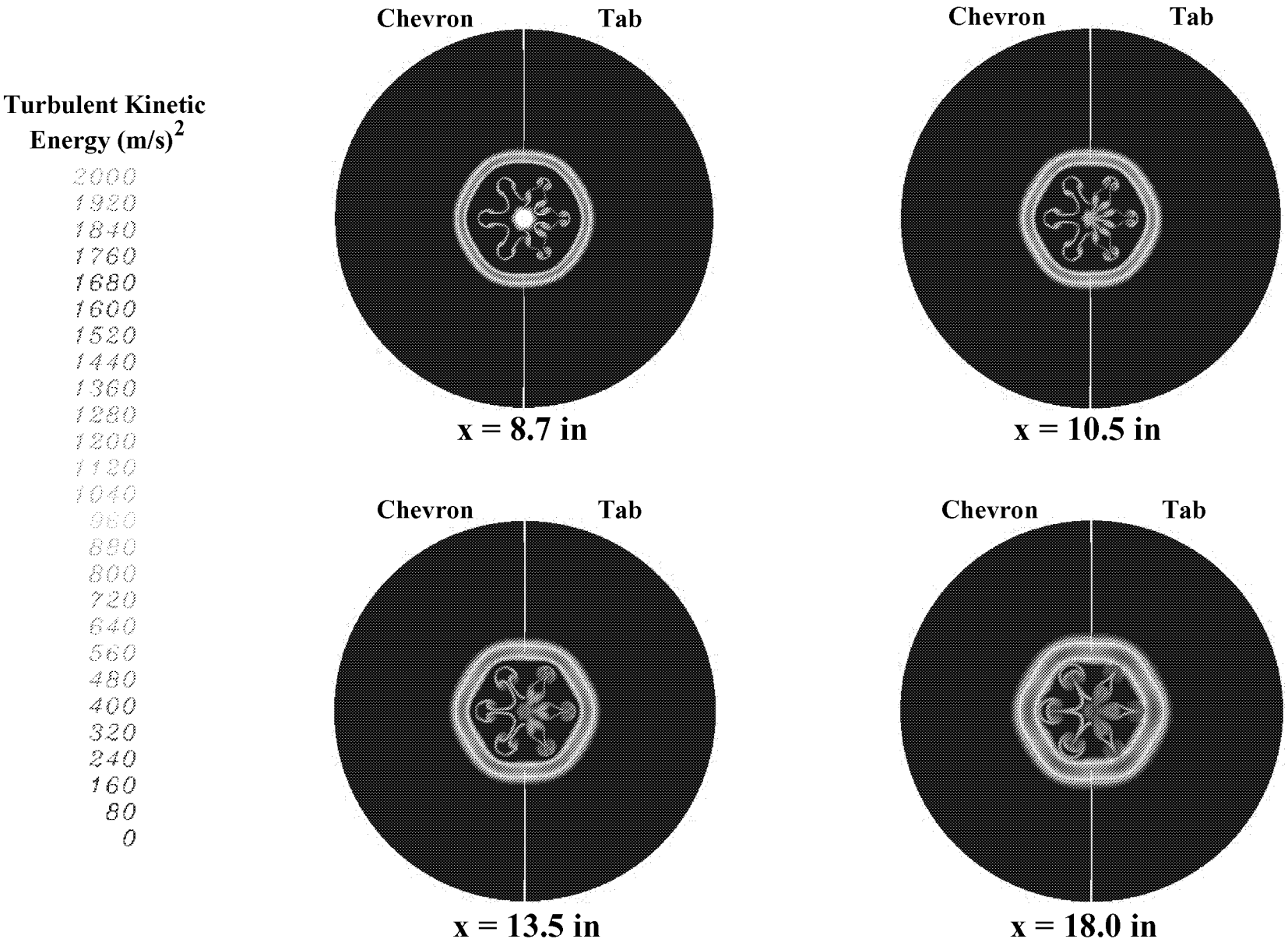

Figure 37. Comparison of turbulent kinetic energy contours (continued).

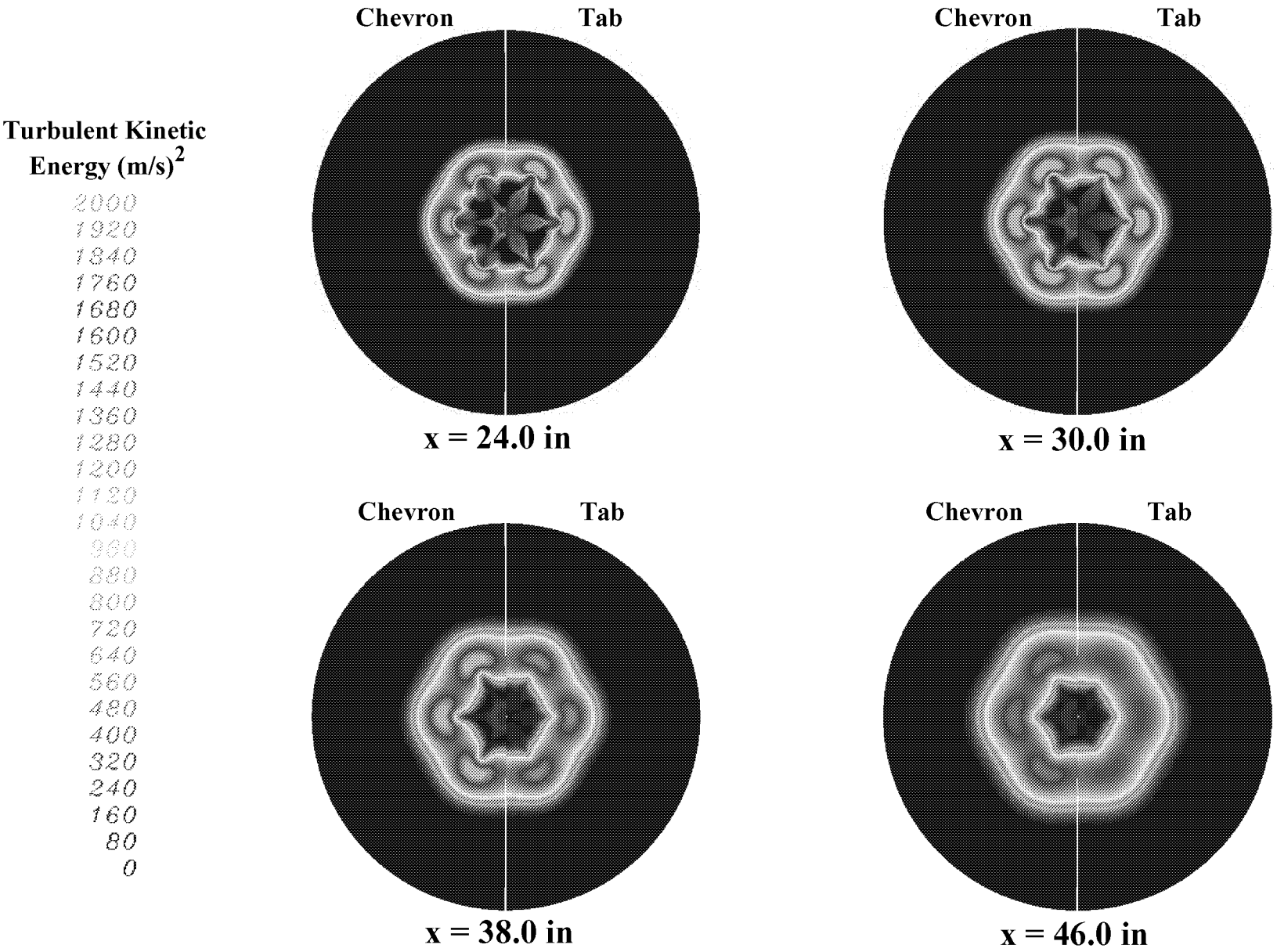

Figure 37. Comparison of turbulent kinetic energy contours (continued).

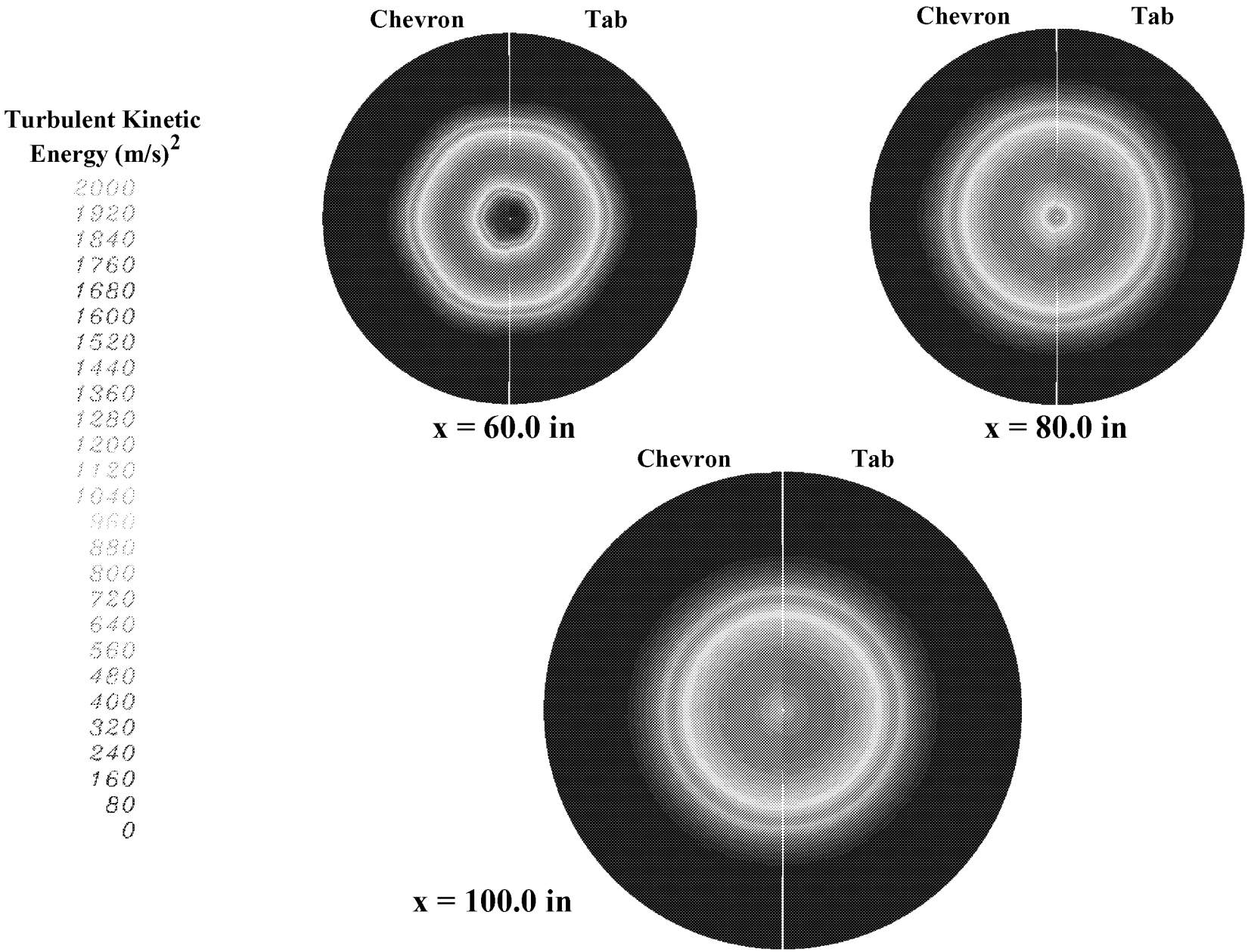

Figure 37. Comparison of turbulent kinetic energy contours (continued).

REPORT DOCUMENTATION PAGE

Form Approved
OMB No. 0704-0188

1. AGENCY USE ONLY (*Leave blank*)	2. REPORT DATE	3. REPORT TYPE AND DATES COVERED
	April 2001	Final Contractor Report

4. TITLE AND SUBTITLE

Task 2—Flow Solution for Advanced Separate Flow Nozzles Response A: Structured Grid Navier-Stokes Approach

5. FUNDING NUMBERS

WU–781–30–12–00
NAS3–99098

6. AUTHOR(S)

D.C. Kenzakowski, J. Shipman, and S.M. Dash

7. PERFORMING ORGANIZATION NAME(S) AND ADDRESS(ES)

Combustion Research and Flow Technology, Inc.
174 N. Main Street, Building 3
P.O. Box 1150
Dublin, Pennsylvania 18917

8. PERFORMING ORGANIZATION REPORT NUMBER

E–12571

9. SPONSORING/MONITORING AGENCY NAME(S) AND ADDRESS(ES)

National Aeronautics and Space Administration
Washington, DC 20546–0001

10. SPONSORING/MONITORING AGENCY REPORT NUMBER

NASA CR—2001-210611

11. SUPPLEMENTARY NOTES

Work was also funded under CRAFT Tech Project No. C069. Project Manager, Naseem Saiyed, Structures and Acoustics Division, NASA Glenn Research Center, organization code 5940, 216–433–6736.

12a. DISTRIBUTION/AVAILABILITY STATEMENT

Unclassified - Unlimited
Subject Category: 71 Distribution: Nonstandard

Available electronically at http://gltrs.grc.nasa.gov/GLTRS

This publication is available from the NASA Center for AeroSpace Information, 301–621–0390.

12b. DISTRIBUTION CODE

13. ABSTRACT ***(Maximum 200 words)***

NASA Glenn Research Center funded a computational study to investigate the effect of chevrons and tabs on the exhaust plume from separate flow nozzles. Numerical studies were conducted at typical takeoff power with 0.28 M flight speed. Report provides numerical data and insights into the mechanisms responsible for increased mixing.

14. SUBJECT TERMS

Acoustic nozzles; Aeroacoustics; Aircraft noise; Engine noise; Exhaust nozzles; Jet aircraft noise; Jet engines; Mixers; Noise reduction; Noise suppressors; Sonic nozzles

15. NUMBER OF PAGES

68

16. PRICE CODE

A04

17. SECURITY CLASSIFICATION OF REPORT	18. SECURITY CLASSIFICATION OF THIS PAGE	19. SECURITY CLASSIFICATION OF ABSTRACT	20. LIMITATION OF ABSTRACT
Unclassified	Unclassified	Unclassified	